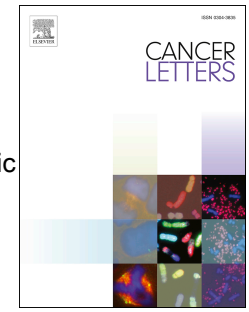

COPZ1 depletion in thyroid tumor cells triggers type I IFN response and immunogenic cell death

Tiziana Di Marco, Francesca Bianchi, Lucia Sfondrini, Katia Todoerti, Italia Bongarzone, Elisa Margherita Maffioli, Gabriella Tedeschi, Mara Mazzoni, Sonia Pagliardini, Sandra Pellegrini, Antonino Neri, Maria Chiara Anania, Angela Greco

PII: S0304-3835(20)30073-2

DOI: https://doi.org/10.1016/j.canlet.2020.02.011

Reference: CAN 114693

To appear in: *Cancer Letters*

Received Date: 10 October 2019

Revised Date: 7 February 2020

Accepted Date: 10 February 2020

Please cite this article as: T. Di Marco, F. Bianchi, L. Sfondrini, K. Todoerti, I. Bongarzone, E.M. Maffioli, G. Tedeschi, M. Mazzoni, S. Pagliardini, S. Pellegrini, A. Neri, M.C. Anania, A. Greco, COPZ1 depletion in thyroid tumor cells triggers type I IFN response and immunogenic cell death, *Cancer Letters*, https://doi.org/10.1016/j.canlet.2020.02.011.

COPZ1 depletion in thyroid tumor cells triggers type I IFN response and immunogenic cell death

Tiziana Di Marco[1], Francesca Bianchi[2], Lucia Sfondrini[3], Katia Todoerti[4], Italia Bongarzone[1], Elisa Margherita Maffioli[5], Gabriella Tedeschi[5,6], Mara Mazzoni[1], Sonia Pagliardini[1], Sandra Pellegrini[7], Antonino Neri[4,8], Maria Chiara Anania[1,*] and Angela Greco[1,*,§]

[1]Molecular Mechanisms Unit, Department of Research, Fondazione IRCCS Istituto Nazionale dei Tumori, Milan, Italy; [2]Molecular Targeting Unit, Department of Research, Fondazione IRCCS Istituto Nazionale dei Tumori, Milan, Italy; [3]Dipartimento di Scienze Biomediche per la Salute, University of Milan, Italy; [4]Hematology Unit, Fondazione IRCCS Ca' Granda, Ospedale Maggiore Policlinico, Milan, Italy; [5]Department of Veterinary Medicine, University of Milan, Italy; [6]Fondazione Filarete, Milan, Italy; [7]Institut Pasteur, Unit of Cytokine Signaling, Inserm U1221, Paris, France; [8]Department of Oncology and Hemato-oncology, University of Milan, Italy.

* Co-last authors.

§ Corresponding author. Fondazione IRCCS Istituto Nazionale dei Tumori, Via G.A. Amadeo, 42, 20133, Milan, Italy. E-mail address: angela.greco@istitutotumori.mi.it (A. Greco).

Tiziana Di Marco, Fondazione IRCCS Istituto Nazionale dei Tumori, Milan, Italy, Via G.A. Amadeo, 42, 20133 Milan, Italy. Tel. 0039 02 2390 5149 tiziana.dimarco@istitutotumori.mi.it

Francesca Bianchi, Fondazione IRCCS Istituto Nazionale dei Tumori, Milan, Italy, Via G.A. Amadeo, 42, 20133 Milan, Italy. Tel. 0039 02 2390 2563 francesca.bianchi@istitutotumori.mi.it

Lucia Sfondrini, University of Milan, Italy, Via G.A. Amadeo, 42, 20133 Milan, Italy. Tel. 0039 02 2390 3780 lucia.sfondrini@unimi.it

Katia Todoerti, Fondazione IRCCS Ca' Granda, Ospedale Maggiore Policlinico, Milan, Italy, Via Francesco Sforza, 35, 20122 Milan, Italy. katiatodoerti@gmail.com

Italia Bongarzone, Fondazione IRCCS Istituto Nazionale dei Tumori, Milan, Italy, Via G.A. Amadeo, 42, 20133 Milan, Italy. Tel. 0039 02 2390 2219 italia.bongarzone@istitutotumori.mi.it

Elisa Margherita Maffioli, University of Milan, Italy, Via Celoria, 10, 20133, Milan, Italy. Elisa.Maffioli@unimi.it

Gabriella Tedeschi, University of Milan, Italy, Fondazione Filarete, Milan, Italy, Via Celoria, 10, 20133, Milan, Italy 0039 02503 18127 gabriella.tedeschi@unimi.it

Mara Mazzoni, Fondazione IRCCS Istituto Nazionale dei Tumori, Milan, Italy, Via G.A. Amadeo, 42, 20133 Milan, Italy. Tel. 0039 02 2390 5149 mara.mazzoni@istitutotumori.mi.it

Sonia Pagliardini, Fondazione IRCCS Istituto Nazionale dei Tumori, Milan, Italy, Via G.A. Amadeo, 42, 20133 Milan, Italy. Tel. 0039 02 2390 2476 sonia.pagliardini@istitutotumori.mi.it

Sandra Pellegrini, Institut Pasteur, Unit of Cytokine Signaling, Inserm U1221, 75724, Paris, France. Tel. 0033 01 40 61 3305 sandra.pellegrini@pasteur.fr

Antonino Neri, Fondazione IRCCS Ca' Granda Ospedale Maggiore Policlinico, Milan, Italy, University of Milan, Italy Via Francesco Sforza, 35, 20122, Milan, Italy Tel. 0039 02503 20420 Antonino.neri@unimi.it

Maria Chiara Anania, Fondazione IRCCS Istituto Nazionale dei Tumori, Milan, Italy, Via G.A. Amadeo, 42, 20133 Milan, Italy. Tel. 0039 02 2390 5149 mariachiara.anania@istitutotumori.mi.it

Angela Greco, Fondazione IRCCS Istituto Nazionale dei Tumori, Milan, Italy, Via G.A. Amadeo, 42, 20133 Milan, Italy. Tel. 0039 02 2390 5149 angela.greco@istitutotumori.mi.it

Abstract

The coatomer protein complex zeta 1 (COPZ1) represents a non-oncogene addiction for thyroid cancer (TC); its depletion impairs the viability of thyroid tumor cells, leads to abortive autophagy, ER stress, UPR and apoptosis, and reduces tumor growth of TC xenograft models. In this study we investigated the molecular pathways activated by COPZ1 depletion and the paracrine effects on cellular microenvironment and immune response. By comprehensive and target approaches we demonstrated that COPZ1 depletion in TPC-1 and 8505C thyroid tumor cell lines activates type I IFN pathway and-viral mimicry responses. The secretome from COPZ1 depleted cells was enriched for several inflammatory molecules and damage-associated molecular patterns (DAMPs). Moreover, we found that dendritic cells, exposed to these secretomes, expressed high levels of differentiation and maturation markers, and stimulated the proliferation of naïve T cells. Interestingly, T cells stimulated with COPZ1-depleted cells showed increased cytotoxic activity against parental tumor cells. Collectively, our findings support the notion that targeting COPZ1 may represent a promising therapeutic approach for TC, considering its specificity for cancer cells, the lack of effect on normal cells, and the capacity to prompt an anti-tumor immune response.

Key words: COPZ1, type I IFN, inflammation, immunogenic cell death, thyroid cancer

1. Introduction

Coatomer protein complex zeta 1 (COPZ1) belongs to the heptameric coatomer protein complex I (COPI), which is involved in assembly of coated vesicles on Golgi membranes, retrograde transport of proteins in the ER-Golgi secretory pathway, endosome maturation, autophagy [1;2], viral infection [3], and lipid homeostasis [4]. Members of the COPI complex have been recently proposed as therapeutic targets in cancer such as COPA for mesothelioma, COPB2 for colorectal cancer, lung adenocarcinoma, cholangiocellular carcinoma, and gastric cancer [5-10].

Few investigations have dealt with the role of COPZ1 in cancer. It has been proposed as a vulnerability for several tumor cell types, i.e. prostate, breast, and ovarian carcinoma; tumor cell dependence on COPZ1 is related to the downregulation of the isoform COPZ2, wherein normal cells are not sensitive to COPZ1 inhibition [11].

We have recently demonstrated that COPZ1 represents a vulnerability also for thyroid cancer (TC), since it is required for the viability of different TC cell lines but not of normal thyrocytes. Moreover, COPZ1 is not mutated in PTC and its expression is only slightly reduced with respect to normal thyroid [12;13]. The evidence that it is essential for tumor but not for normal cells, and the absence of mutation or aberrant expression in tumors, renders COPZ1 as a good example of non-oncogene addiction [14] for TC cells.

TC represents the most frequent endocrine cancer, with a rapidly increasing incidence in recent years [15]. The majority of TC originates from epithelial cells and includes well differentiated papillary (PTC) and follicular (FTC) carcinoma, poorly differentiated (PDTC), and undifferentiated anaplastic carcinoma (ATC). Most thyroid cancers are effectively curable by thyroidectomy, thyroid-stimulating hormone suppression, and ablation of residual tissue using radioactive iodine 131 (RAI) [16], with an excellent prognosis consisting of an overall survival rate of 85% at 10 years [17]. However, local recurrence occurs in up to 20% of patients and distant metastases, found in approximately 10% of patients at 10 years, are incurable since they poorly concentrate RAI. Furthermore, patients with PDTC and ATC have unfavourable prognosis, with

survival reduced to a few months after diagnosis for ATC [18;19]. Even though much progress has been made in the treatment of thyroid cancer thanks to the development of a variety of molecular-targeted agents [16], no effective therapeutic options are available for patients with advanced thyroid cancer that is resistant to therapy, indicating the need for new intervention strategies.

We have recently proposed COPZ1 as a therapeutic target for thyroid carcinoma. COPZ1 depletion affects the viability of thyroid tumor cells, and this is associated with abortive autophagy, ER stress, unfolded protein response (UPR), and apoptosis [13]. Moreover, local treatment with siRNA oligos targeting COPZ1 reduces tumor growth of TC xenograft models [13]. Even though we partially elucidated the mechanisms and pathways that are activated in tumor thyroid cells upon COPZ1 depletion, herein we aimed at investigating the cross talk between cell death and tumor microenvironment, focusing on the effects on immune response.

Type I IFN represents the first host defence mechanism against viral infections, and also contributes to innate and adaptive immune responses [20]. Type I IFN expression is rapidly and transiently triggered upon recognition of specific pathogen-associated molecular patterns (PAMPs), mainly nucleic acids, associated with infectious agents, and by damage-associated molecular patterns (DAMPs) derived from stressed or dying cells [21]. A large body of evidence shows that these danger signals share a common key homeostatic process that involves the ER and its response to stress stimuli [22;23].

Since COPZ1 silencing causes ER stress in thyroid tumor cells [13], we investigated in depth these issues, focusing on the activation of the type I IFN response, and its paracrine effects on cellular microenvironment and immune response. On this basis, targeting COPZ1 might share the efficacy of several therapeutic strategies, such as chemotherapy and radiotherapy, which relies on ER stress and type I IFN production in promoting growth inhibition of tumor cells and anti-tumor immune responses [22;24].

2. Materials and methods

2.1 Cell lines and conditioned media

TPC-1 and BCPAP (papillary thyroid carcinoma), and 8505C (anaplastic thyroid carcinoma) cells were obtained from Prof. A. Fusco (University Federico II, Naples, IT); Nthy-ori 3–1 cell line (SV-40 immortalized normal human thyroid follicular cells) was purchased from European Collection of Cell Cultures (ECACC) (Salisbury, UK); THP-1 cells (acute monocytic leukemia) were purchased from ATCC (Manassas, VA, USA). Cells were cultured as reported in [12;25]. Thyroid cell lines were genotyped at the Fragment Analysis Facility of Fondazione IRCCS Istituto Nazionale dei Tumori, using Stem Elite ID System (Promega Corporation, Madison, USA) according to the manufacturer's instructions and ATCC guidelines. The profiles obtained matched to their original profiles [26;27]. Mycoplasma contamination was tested periodically and was negative in all cell lines (PCR Mycoplasma Detection Set, TAKARA Bio Inc). Conditioned media (CM), obtained by incubating subconfluent cultures for different times after siRNA transfection, were collected, centrifuged, passed through 0.20 μm filters, and stored at - 80 °C until use.

2.2 siRNA transfection

siRNA transfection was performed using 20 nM of siRNA oligos (siCOPZ1:MISSION esiRNA EHU1040461, siRNA Universal Negative Control #1 SIC001, Sigma-Aldrich, St. Louis, MO, USA) and the Lipofectamine RNAiMAX reagent (Invitrogen Life Technologies, Carlsbad, CA, USA), according to manufacturer's instructions. Where indicated, cells were transfected with siRNA oligos targeting COPZ1 (4457308, Ambion® ID s22427, Thermo Fisher Scientific, Waltham, MA USA) and with non-targeting oligos (4457289, Ambion® In Vivo Negative Control #1 siRNA) as a control.

2.3 RNA extraction and Gene Expression Profiling

Total RNA samples were extracted using the NucleoSpin®RNA isolation kit (Macherey-Nagel, Duren, Germany). RNA samples were processed for assessing COPZ1 silencing by Real Time PCR (see paragraph 2.5) and for global gene expression profiling (GEP) with GeneChip® Human Gene 2.0 ST arrays (Affymetrix Inc., Santa Clara, CA), according to the manufacturer's instructions. Normalized expression values and annotation were obtained as previously described [28]. Most variable transcripts out of 18 642 specific genes across the entire panel were analyzed by applying hierarchical agglomerative clustering using Pearson's correlation and average linkage methods, using DNA-Chip Analyzer software [29], as previously reported [30]. Supervised analyses were carried out as stated in [31]. The resulting list of differentially expressed genes was investigated using the Database for Annotation, Visualization and Integrated Discovery (DAVID) 6.8 tool (https://david.ncifcrf.gov/). Functional annotation clustering was performed on Gene Ontology (GO), Biological Process (BP), Molecular Function (MF) and Cellular Components (CC) terms at high classification stringency and significant annotation clusters (Enrichment Score, ES> 2) were selected and representative GO terms. Global functional annotation studies were performed in TPC-1 cells, at 72 h after siRNA transfection, using the Gene Set Enrichment Analysis (GSEA) [32] on KEGG, Reactome and Hallmark gene set collections (v 6.2), respectively (nominal p-value <0.05 and FDR q-value < 5%, after 500 gene set permutations). Data have been deposited in Gene Expression Omnibus (GEO) database and are accessible under GSE133485 number.

2.4 Nano-scale LC-MS/MS analysis

Samples were managed and analyzed following the methodology used in [33]. An ANOVA test (false discovery rate 0.05) was carried out to identify proteins that were differentially in siNT and siCOPZ1 cells at 48 h. Differential expression was considered as significant if a protein was present only in siNT or siCOPZ1 cells or its normalized intensity (according to the LFQ algorithm) resulted in a significant difference, as calculated by Welch's t-test (FDR 0.05). The MS proteomics data have been deposited in the ProteomeXchange Consortium via the PRIDE partner repository

[34]. Pathway enrichment analysis was performed using The Molecular Signatures Database (MSigDB) collection (http://software.broadinstitute.org/gsea/msigdb/index.jsp) using Reactome gene sets. Gene sets with an FDR < 0.05 were considered significant. The Search Tool used for the prediction of protein–protein interactions focusing on experimentally verified protein-protein interactions was ToppCluster (https://toppcluster.cchmc.org/) [35]. Proteomic data have been deposited in the ProteomeXchange Consortium via the PRIDE partner repository with the dataset identifier PXD014423.

2.5 Real-time PCR

RNA was extracted as described above and reverse transcriptase-PCR was performed as previously described [36]. For real-time PCR analysis 20 ng of retrotranscribed RNA were amplified in PCR reactions carried out in triplicate on an ABI PRISM 7900 using the following TaqMan gene expression assays (Applied Biosystem, Foster City, CA): Hs01023197_m1 (COPZ1), Hs01061436_m1 (DDX58), Hs01675197_m1 (IFIT1), Hs00895608_m1 (MX1), Hs00242943_m1 (OAS1), Hs01013996_m1 (STAT1), Hs00185375_m1 (IRF7), Hs00192713_m1 (ISG15), Hs01551078_m1 (TLR3), Hs02800695_m1 (HPRT1), used as a housekeeping gene for normalization among samples. Expression of immune-inflammatory related genes (Supplementary Table I) was analyzed by a customized TaqMan Low Density Array (Applied Biosystems) using 2 ng of retrotranscribed RNA as template. Data analysis was performed using SDS (Sequence Detection System) 2.4 software.

2.6 Western blot analysis

Western blot analysis was performed as previously described [36], using the following antibodies: anti-RIG-1 (sc-376845 (D-12), anti-COPZ1 (sc-398081 (B-12) from Santa Cruz Biotechnology, Inc. (Dallas, TX, USA); anti-MX1 (37849S), anti-p-STAT1 (7649), anti-p-TBK1/NAK (5483), anti-TBK1/NAK (51872) from Cell Signaling Technology Inc (Danvers,

MA,USA); anti-STAT1 (610186) from BD Biosciences (San Jose, CA, USA); anti-IL6 (ab6672), anti-IL8 (ab18672), anti- IL1β (ab9722), anti-calreticulin (ab92516), anti-HMGB1 (ab18256) from Abcam (Cambridge, UK); anti-γH2AX (A300-081A-M) from Bethyl Laboratories (Montgomery, TX, USA); anti-β-actin (A2066) from Sigma-Aldrich, (St Louis, Mo, USA). Membranes were stained with Ponceau S solution (Sigma-Aldrich) before antibody incubation for checking protein loading.

2.7 ATP assay

Extracellular ATP levels were measured in conditioned media using the bioluminescence Molecular Probes® ATP Determination Kit (A22066) (ThermoFisher Scientific, Waltham, MA USA) according to the manufacturer's instructions. Luminescence was measured on a microplate reader (TecanUltra, Tecan Trading AG, Switzerland).

2.8 Enzyme-linked immunosorbent assay (ELISA)

Quantification of cytokines in conditioned media was performed by commercially available ELISA according to the manufacturer's instructions: IFNβ (DIFNB0), CXCL10 (DIP100) from R&D Systems (Space Import, Milan, Italy); IL1α, IL1β, IL2, IL4, IL5, IL6, IL8, IL10, IL12, IL13, IL17α, GM-CSF (Multi-Analyte ELISArray Kit MEH-0066 (336161) from Qiagen Sciences (Maryland, USA). Cytokine levels were determined by evaluating absorbance at 450 nm on a microplate reader (TecanUltra, Tecan Trading AG, Switzerland).

2.9 Flow cytometry

In order to detect surface calreticulin, cells were harvested and incubated for 15 min with the zombie dye (Zombie Aqua™ Fixable Viability Kit (423102) BioLegend San Diego, CA, USA) to assess live vs. dead cells. Cells were then washed and incubated for 30 min with the anti Alexa Fluor® 488 conjugate calreticulin antibody (#62304, (D3E6) or isotype control (#2975, DA1E)

(Cell Signaling Technology Inc, Danvers, MA, USA) following the manufacturer's instructions. Cells were then analyzed with a BD FACSCanto™ instrument (BD Biosciences San Jose, CA, USA). The gating strategy is provided in Supplementary Fig. S4.

2.10 Maturation of THP-1 on dendritic cells

THP-1 cells were cultured as reported in [25] to obtain a population of immature dendritic cells (iDCs). Briefly, THP-1 cells were seeded at a concentration of 1.75 x 10^5 cells/mL in 10% FBS-RPMI 1640 containing 100 ng/mL GM-CSF (Peprotech, RockyHill, CT, USA) and 100 ng/mL IL-4 (Sigma-Aldrich, St Louis, Mo, USA). THP-1 cells were cultured for 5 days and the medium was replaced every two days. iDCs were then cultured for supplementary 3 days in 50% of CM from siCOPZ1 or siNT TPC-1 cells, harvested 72 h after siRNA transfection. As a positive control for DC maturation, iDCs were cultured for 3 days in 10% FBS-RPMI 1640 containing 100 ng/mL GM-CSF, 200 ng/mL IL-4, 20 ng/mL TNF-α (Sigma-Aldrich) and 200 ng/mL ionomycin (Calbiochem, Merck, Germany). DCs were assessed by FACS for expression of differentiation and maturation markers [37] using the following antibodies: PE Mouse Anti-Human CD11c and BB700 Rat Anti-CD11b, BB515 Mouse Anti-Human CD80, BV650 Mouse Anti-Human CD86, BV421 Mouse Anti-Human CD83, APC Mouse Anti-Human HLA-DR (BD, Biosciences., San Jose, CA, USA). Cells were analyzed with a BD FACSCelesta™ instrument (BD Biosciences) and FlowJo software (TreeStar, Ashland, OR, USA).

2.11 *Ex vivo* isolation of T-cells and proliferation assay

Human T cells were isolated by negative selection with the Dynabeads untouched human T cells (11344D, Thermo Fisher Scientific, Waltham, MA USA) from the leukocyte-rich component (buffy coat) of blood healthy donors using a protocol approved by the Ethics committee of the Fondazione IRCCS Istituto Nazionale dei Tumori, Milan, Italy. An informed consent was obtained from all donors. Cells were then labeled with CFSE (Cell Trace CFSE Cell Proliferation Kit,

Thermo Fisher Scientific) according to the manufacturer's recommendations, and cultured for 4 days in complete RPMI 1640 at 1×10^5 cells/well in 96-well U-bottom plates in the presence of anti CD3/CD28 Dynabeads (11132D, Thermo Fisher Scientific) and 50% CM from DCs pulsed with CM from TPC-1 silenced for COPZ1 or control. Proliferation of T cells was evaluated after 4 days of culture, when two clearly distinct fractions of proliferating (CFSE-"low") and non-proliferating (CFSE-"high") were detectable. Just before analysis, cells were stained with BV786 Mouse Anti-Human CD3 antibody (BD Biosciences, San Jose, CA, USA) for 25 min on ice. Flow cytometric analysis was performed using a FACSCelesta™ instrument (BD Biosciences, San Jose, CA, USA) and FlowJo software (TreeStar, Ashland, OR, USA).

2.12 *In Vitro* Cytotoxicity Assay

T cell-mediated cytotoxicity was determined by ^{51}Cr release assay. Briefly, TPC-1 cells, 48 h after siRNA transfection, were exposed to 1 Gy of irradiation delivered as a single dose using the ^{137}Cs γ-irradiator IBL-437 (dose rate 5.2 Gy/min), and and co-cultured for 6 days with PBMCs derived from buffy coats of blood healthy donors. Then, media were harvested and processed for T cell isolation as described above. For the cytotoxicity assay, parental TPC-1 cells were labeled with 100 μCi ^{51}Cr (Perkin-Elmer, Waltham, MA, USA) for 1 h at 37°C, washed 3 times with PBS-5% FCS, and resuspended in DMEM, containing 10% FBS. T cells were then co-incubated with ^{51}Cr-labeled TPC-1 cells at a target: effector ratio of 1:50 and 1:100 in triplicate in 96-well U-bottomed plates for 4 h at 37°C. The radioactivity in the supernatant (100μl) was measured on a Trilux Beta scintillation counter (PerkinElmer, Waltham, MA, USA). Percentage specific lysis was calculated as: 100 x (experimental Counts per Minute (cpm)- spontaneous cpm)/(maximum cpm-spontaneous cpm).

2.13 Statistical analysis

All statistical analyses were performed using GraphPad Prism software (version 5.02). Groups were compared using the two-tailed unpaired/paired Student's *t*-test and non parametric Wilcoxon test. *P*-values < 0.05 were considered significant.

3. Results

3.1 Gene expression profiling of COPZ1-depleted thyroid cancer cells

We characterized the transcriptional landscape in thyroid cancer cells depleted of COPZ1. In details, we performed a global gene expression profiling (GEP) by microarray analysis comparing COPZ1-depleted (siCOPZ1) and control (siNT) TPC-1 (papillary thyroid tumor cell line) at 48 h and 72 h post-siRNA transfection. The same analysis was performed in Nthy-ori 3-1 (immortalized normal human thyrocytes), whose growth is not affected by COPZ1 silencing [12;13]. Hierarchical clustering of the 857 most variable genes across the entire dataset revealed very similar gene expression patterns in normal thyrocyte samples, irrespective of COPZ1 silencing. TPC-1 samples at 72 h of COPZ1 depletion were grouped in a sub-cluster, distinct from 48 h COPZ1-silenced or control siNT samples (Fig. 1A). In order to define patterns potentially associated with COPZ1 depletion in thyroid tumor cells, COPZ1-silenced TPC-1 cells were compared to siNT control at both time points. Supervised analysis by Significant Analysis of Microarray (SAM) software identified 99 significantly differentially expressed genes, almost all (97%) of which were up-regulated, whereas 6 genes, including COPZ1 as expected, were down-regulated (Fig. 1B and Supplementary Table II). Functional annotation clustering by DAVID 6.8 was applied on the identified gene list, thus showing 17 significant annotation clusters associated with unfolded protein response, protein transport or localization, vesicle coating and transport, regulation of cytokine production or apoptotic pathway (Table I). On the contrary, no peculiar gene expression profiles were observed in COPZ1-silenced Nthy-ori 3-1 cells vs. control (data not shown).

Additionally, to identify *a priori* defined sets of genes showing a concordant modulation in silenced vs control phenotypes, Gene Set Enrichment Analysis (GSEA) was applied on global gene expression profiles of TPC-1 72 h post-transfection by interrogating different collections of gene sets (KEGG, Hallmark, Reactome) (Supplementary Table III). Several up-regulated gene sets, most of them already modulated at 48 h post-transfection, resulted significantly associated with unfolded

protein response, DNA replication, cell cycle regulation, chromosome maintenance, spliceosome components, inflammatory response, and cytokine signaling pathways.

The enrichment plots of selected top significant gene sets are shown in Fig. 1C, and the corresponding gene lists are reported in Supplementary Table IV. These results indicate that, at the transcriptional level, COPZ1 silencing is strongly associated with ER stress and the onset of an inflammatory response.

3.2 Proteome analysis of COPZ1-depleted thyroid cancer cells

To characterize deregulated proteins and gain information on potential adaptive responses and stress pathways in COPZ1-depleted TPC-1 cells, we performed label-free quantitative proteomic analysis of total proteins at 48 h post-siRNA transfection. We found a total of 2 057 proteins and ANOVA test (FDR < 0.05) was carried out to identify proteins that were differentially expressed between siNT and siCOPZ1 samples. The Venn diagram in Fig. 2A shows that 177 proteins were differentially expressed in siCOPZ1 cells, of which 97 were down-regulated and 80 up-regulated. A subset of 124 proteins was exclusively detected in siNT cells and a subset of 148 proteins was exclusively found in siCOPZ1 cells. The Volcano plot in Fig. 2B shows the differentially expressed proteins based on fold change *vs* t-test probability (Welch difference). Interestingly, among the top significant upregulated proteins, we found: H2AX, involved in DNA repair, replication and chromosomal stability, transcription regulation, whose increased expression has been also documented by western blot (Fig. S1); ISG15 and MAVS (mitochondrial antiviral signaling), both involved in innate response to viral infection.

Using the Molecular Signature Database from GSEA website, we interrogated gene sets derived from the Reactome pathway database, considering the proteins expressed at the highest levels (80 plus 148) in COPZ1-silenced TPC-1 cells. Among the up-regulated pathways (FDR q-values < 0.05), functions related to the immune system, immune cytokine signaling, and interferon signaling were found to be over-represented (Fig. 2C). In order to reveal potential hidden relations

between pathway members, we performed a network analysis using some of the significant Reactome pathways as input and TOPPcluster software, considering enriched terms from Gene Ontology and pathways.

As summarized in Fig. 2D, the proteomic profiling of COPZ1-silenced TPC-1 cells highlighted deregulated proteins and functional networks related to response to stress and cytokines, innate immune response, type I IFN signaling, and regulation of viral life cycle.

3.3 COPZ1 depletion activates the type I interferon response

The results described above suggest that COPZ1 silencing may prompt an inflammatory program, possibly mirroring a viral infection that involves the type I IFN pathway. To test this issue, we measured the expression of the Toll-like receptor 3 (TLR3), as well as selected genes that exert a pivotal role in response to infection, in both COPZ1-depleted TPC-1 and 8505C (anaplastic thyroid carcinoma) cells. Real-time PCR showed that *TLR3* transcript levels were increased in both COPZ1-silenced cell lines vs. controls. A similar trend was seen for *DDX58, MX1, OAS1*, and several IFN stimulated-genes (ISGs), such as *STAT1, IRF7,* and *ISG15* (Fig. 3A). Western blot documented a strong increase in protein levels of RIG-1 (retinoid acid-inducible gene I, encoded by *DDX58*) and MX1 (Myxovirus resistance protein 1), a dynamin like GTPase protein with a broad antiviral activity (Fig. 3B). TLR3 and RIG-1, through the involvement of adaptor molecules such as TRIF and MAVS, respectively, activate TBK1 (TANK-binding kinase 1), which mediates phosphorylation and activation of the transcription factors IRF3 and IRF7, and NF-kB, required for IFNβ production [38]. In line with the activation of these sensors, we observed an increased level of Ser^{172}-pTBK1 (Fig. 3D). To obtain a broader view of the effect of COPZ1 silencing on type I IFN response genes, we performed gene expression analysis using a customized TaqMan Low Density Array containing 40 genes related to this pathway, including six of seven genes in Fig. 3A. Interestingly, COPZ1 silencing led to an increase in the level of several ISG transcripts, such as *MX1, MX2, NF-kB, OAS1, OAS3, OASL, STAT1, STAT2, IFIH1, IFIT1, IFIT2, IFNB1, IRF1, IRF3,*

and *IRF7* (Fig. 3D, Fig.S2C). Similar results were obtained in an additional PTC-derived cell line, namely BCPAP (Fig. S3C).

3.4 COPZ1 depletion is associated with type I IFN-induced inflammation

Activation of IRF3/NF-kB leads to secretion of IFNβ, which activates the JAK/STAT signaling pathway, triggering autocrine and paracrine circuitries resulting in production of IFNs, induction of ISGs, and the release of inflammatory molecules [39]. Indeed, high levels of IFNβ in both COPZ1-silenced TPC-1 and 8505C cell cultures were measured by ELISA, which were undetectable or very low in siNT cells (Fig. 4A). Moreover, the levels of Tyr^{701}-pSTAT1 and total STAT1 were increased in COPZ1-silenced cells (Fig. 4B). Since type I IFN induces the transcription of pro-inflammatory molecules, we analyzed the cytokine/chemokine mRNA profiles using a TaqMan Low Density Array scoring 36 genes mainly involved in inflammation. Notably, in both COPZ1-silenced cell lines, we observed strong upregulation of genes encoding for inflammatory cytokines and chemokines, among which the inflammatory cytokines IL-1α, IL-1β, IL-6, TNFα, and CCL5/RANTES, and the chemotactic factors CXCL1, CXCL8, CCL20, CCL3, and GM-CSF (Fig. 4C, Fig. S2C). Using a multi-analyte ELISA assay, we characterized the secretome of COPZ1-depleted tumor cells, focusing on a panel of cytokines known to be involved in inflammatory processes. In accordance with what observed at the transcriptional level, a marked increase of IL-1α, IL-1β, IL-6 and GM-CSF was found in both COPZ1-depleted cell lines (from 20 to 70 fold vs. control) with some differences between the two cell lines (Fig. 4D). The presence of IL-1β, IL-6, and IL-8 in secretomes was further confirmed by western blot (Fig. 4E, Fig. S2D), also in BCPAP cells (Fig. S3D). It is known that type I IFN can induce CXCL10, an essential chemokine responsible for the recruitment of anti-tumor immune cells [40]. Indeed, we found that silencing of COPZ1 induced accumulation of the *CXCL10* transcript (Fig. 4C), and a CXCL10 secretion as assessed by ELISA (Fig. 4F).

All together, these studies revealed marked increased expression and secretion of several pro-inflammatory molecules in cells depleted of COPZ1.

3.5 COPZ1 silencing is associated with immunogenic cell death

The link between the type I IFN pathway and immunogenic cell death (ICD) is well established [41]. A key feature of ICD is the rapid surface exposure of calreticulin (ecto-calreticulin), early secretion of ATP, and the release of proteins such as high mobility group box 1 (HMGB1), all known as damage-associated molecular patterns (DAMPs) [42]. To assess whether cell death induced by COPZ1 depletion promotes production of DAMPs, we silenced COPZ1 in TPC-1 and 8505C cells and monitored surface exposure of calreticulin by flow cytometry in time-course experiments. For both siNT cell lines, the majority of cells, which were essentially alive over time, poorly expressed ecto-calreticulin (CRT). In contrast, in COPZ1-depleted cells, a consistent increase in percentage of viable cells expressing ecto-calreticulin (from 6.13 to 29.40% for TPC-1 and from 0.56 to 46.1% for 8505C) was observed, with a concomitant decrease of viable cells, as expected by COPZ1 depletion (Fig. 5A). As reported in Fig. 5B, the overlay histogram plots showed a consistent increase of the mean fluorescence intensity in COPZ1-depleted cells as compared to the control. The gating strategy to analyze ecto-CRT expression is reported in Fig. S4.

Of note, in the conditioned medium (CM) from COPZ-1 silenced cells, calreticulin and HMGB-1 were strongly increased at 72 h, even though the amount of the protein in total extracts remained constant (Fig. 5C, Fig. S2D). Similar results were obtained in COPZ1-depleted BCPAP cells (Fig. S3D). As shown in Fig. 5D, COPZ1-depleted cells also secreted higher amounts of ATP in comparison to control cells.

These results indicate that thyroid tumor cells produce DAMPs upon depletion of COPZ1.

3.6 COPZ1-induced cell death promotes dendritic cell maturation and cytotoxic T cell response

The production of DAMPs by COPZ1 depleted cells indicates the occurrence of ICD. We next investigated whether COPZ1-depleted cells have the ability to stimulate and activate innate immune cells, notably dendritic cells (DCs), which have the potential to cross prime adaptive immune responses (mainly T cells) [43]. For this purpose, we first investigated the effect of CM from COPZ1-depleted cells, enriched with DAMPs, to promote DC maturation *in vitro*. Immature DCs (iDCs) were derived from THP-1 cells (acute monocytic leukemia) and were exposed for 3 days to CM obtained 72 h after transfection of TPC-1 cells with siCOPZ1 or siNT oligos. As a positive control for expression of maturation markers, a fraction of iDCs was cultured with appropriate maturation stimuli [25]. FACS analysis revealed that, similar to cells exposed to maturation-inducing stimuli, iDCs cultured in the presence of CMs up-regulated CD11b and CD11c, which are markers of DC lineage (Fig. 6A). Analysis of the expression of CD80, CD83, CD86, and HLA-DR maturation markers revealed an up-modulation of all these markers on iDCs exposed to CM from siCOPZ1-TPC-1 cells compared to iDCs exposed to CM from siNT-TPC-1 cells (Fig. 6B and C). Similar effects were observed when CM from COPZ1-silenced 8505C cells was used (data not shown). Graphical explanation of the experimental procedure is shown in Figure 6D.

These *in vitro* results suggest that COPZ1-depletion induce the release of factors that promote DC maturation.

Next, we investigated whether DCs, pulsed with CM from COPZ1-silenced cells, were able to stimulate the proliferation of freshly isolated naïve $CD3^+$ T cells. T cells were labeled with CFSE, cultured in the presence of CM from pulsed DCs, stimulated with anti-CD3/anti-CD28 beads, and assessed by FACS for proliferation 4 days later. The proportions of $CD3^+$ T cells at each cell division (from gate 1 to 4) was compared between samples cultured in the presence of CM from DCs pulsed with CM from siCOPZ1- or siNT TPC-1 cells. A significant difference was found between the percentage of cells in gate 1 ($CFSE^{high}$) and gate 4 ($CFSE^{low}$) (Fig. 7A). Specifically, as shown in Fig. 7B, a significantly higher percentage of $CD3^+$ T cells was detected in $CFSE^{low}$ gate 4

in cultures incubated with CM from DCs treated with COPZ-1-silenced CM than those incubated with DCs treated with NT-silenced CM. Conversely, a lower percentage of $CD3^+$ T cells was detectable in $CFSE^{high}$ gate 1 in COPZ1-silenced versus siNT samples.

To explore if COPZ1-silenced cells might trigger an immune activation that would result in the killing of parental cells, PBMCs derived from healthy donor were incubated for 6 days with TPC-1 cells, transfected with siCOPZ1 or siNT oligos 48 h before . T cells were then purified from PBMC s collected from co-cultures and co-incubated for 4 h with ^{51}Cr-labeled parental TPC-1 cells. Interestingly, T cells from COPZ1-silenced cell stimulation exerted a significant increased cytotoxic activity as compared to T cells from siNT-silenced cells (Fig. 7D). Experiments reported above are graphically represented in Fig. 7C and 7E.

Together, these findings indicate that cell death induced by COPZ1 silencing promotes immune events that culminate in the killing of parental tumor cells.

4. Discussion

Despite considerable progress in the genetic and molecular characterization of thyroid carcinoma, few or no therapeutic options are currently available for patients with aggressive and iodine-refractory thyroid tumors. Thus, there is a need to identify new treatment strategies. Towards this aim, we had previously identified COPZ1 as a non-oncogene addiction for thyroid tumor cells, since its silencing induces cell death in several tumor cell lines, regardless of histotype or specific genetic lesions, but not in normal cells [12]. Thus, COPZ1 targeting may represent a novel therapeutic approach for thyroid cancer. The development of selective small molecules may be useful to improve its translational relevance not only for thyroid cancers, but also for different tumor types sensitive to COPZ1 inhibition [11].

We recently described that COPZ1 depletion in thyroid tumor cells leads to abortive autophagy, ER stress, UPR, and cell death [13]. These latter processes are known to evoke a type I IFN-mediated pro-inflammatory response, similar to that induced by radiotherapy or specific chemotherapy agents, which can stimulate an immune response. To explore this possibility, in this study we performed gene expression profiling and proteomic analysis of COPZ1-depleted thyroid tumor cells. By integrating these approaches, we highlighted the involvement of pathways related to ER stress and type I IFN-mediated inflammation. Of note, a chronic activation of the type I IFN response has been reported in inherited autoimmune disorder COPA syndrome [44], caused by mutations of the coatomer complex member COP-α, which impair ER-Golgi transport, increase ER stress, activate UPR, and upregulate cytokines [45;46].

With the aim to better unravel key players involved in the mechanisms reported above, we first found that COPZ1 silencing leads to increased levels of TLR3 and RIG-1 which, after activation by double-stranded RNAs, trigger signaling cascades that ultimately result in the production of type I IFNs [38;47]. We also detected the up-regulation of several ISGs, activation of TBK1 and increased levels of IRF3/7, all involved in IFNβ gene induction. Indeed, we observed that COPZ1 depletion leads to the production of IFNβ, a key innate cytokine which, as the other

type I IFNs, can limit tumor cell proliferation, drive senescence and apoptosis, amplify inflammation and exert an anti-tumor activity [48-50].

Since activation of UPR is known to connect ER function to “altered-self mimicry”, mainly through the generation of dsRNA fragments [51;52], we hypothesize that this may also occur when in thyroid cancer cells the ER stress is induced by COPZ1 depletion, thus mirroring a viral infection. Even though this pathway is generally induced by cytoplasmic dsRNA fragments, other signals starting from DNA damage may lead to TLR3 activation and TLR3-dependent cytokine secretion [53], even if the mechanisms are still unclear. Thus, we cannot exclude that in our setting the source of nucleic acids is DNA that has been damaged as a consequence of ER stress [54]. Several lines of evidence support this possibility: 1) gene expression and proteomic profiling highlighted the presence of DNA damage and chromatin remodeling in COPZ1-depleted cells; 2) accumulation of γH2AX, a well-known marker of DNA damage, was assessed by proteomic analysis and by western blot; 3) COPZ1 has been identified as a key player in mediating genome stability, since its silencing induces DNA damage [55]. Further studies will need to assess whether an aberrant cytosolic accumulation and type of nucleic acids occur in our model.

ER stress and UPR are known to promote signaling events leading to the production of pro-inflammatory products [56]. We found a significant increase of cytokines, including IL-1β, IL-6, and IL-8, which are known to be pro-tumoral in some circumstances, but to have in others potent immune modulatory functions, such as induction of MHC class I on DC, promotion of T cell differentiation/survival, and activation of NK cells [57]. Moreover, we found a significant increase in the production of a number of ISGs molecules such as CCL5, CCL3, CCL20, and CXCL10, which are potent chemo-attractants to lymphocytes and monocytes [21;40]. Even though most of the inflammatory cytokines and chemokines produced by COPZ1-depleted cells are considered pro-tumoral, also in the context of thyroid tumors [58-60], we cannot exclude that the opposite effect may occur depending on intensity of the signal and of microenvironmental cues.

Cell death occurring in the context of UPR can elicit an immune response through the release of endogenous danger signals. In our model, we found that COPZ1-depleted cells initiate an IFN/viral mimicry response and succumb to ICD, which, in turn, amplifies inflammation and cell death. Indeed, we detected several secreted DAMPs such as calreticulin, HMGB1, and ATP, but also IL-1α, IL-1β, IL-6, and IFNβ, exerting a key role on orchestrating ICD-related events and typically promoted by ICD inducer agents [57]. We should also consider that COPZ1 silencing induces apoptotic cell death [13], with supposedly the release of ss/dsDNA, dsRNA and mitochondrial DNA, which, by acting as DAMPs, can activate TLR- or RIG-1-like receptors in a paracrine manner. This may also in part sustain the activation of the related pathway, previously described.

We found that the secretome of COPZ1-depleted cells is able to induce maturation of DCs and, in turn, T cell activation, a mechanism known to be triggered by cytokines like IL-1β, IL-6, IL-12 and TNFα [57]. In our model, these phenomena may be also ascribed to the production of IFNs, known to be potent immune modulators by acting on DC, by decreasing the suppressive function of both regulatory T cells and myeloid-derived suppressor cells, although in certain circumstances, opposite effects responsible for evasive mechanisms and promotion of tumor progression have been reported [48;61;62]. Our results revealed that T cells, isolated from PBMCs stimulated by COPZ1-depleted thyroid tumor cells increased their ability to *in vitro* lyse parental cells, suggesting that COPZ1 depletion in tumor cells might trigger a chain of immunological events that would result in the immunological recognition of structures expressed by the parental tumor cells.

To assess the effect of COPZ1 depletion on cell-mediated immunity and inflammation, and the translational value of our *in vitro* results, *in vivo* experiments in *ad hoc* immunocompetent murine models are needed. They are also necessary to: i) clearly define whether COPZ1 silencing represents a strategy to establish a specific CTL-mediated anti-cancer immune response; ii) evaluate whether may contribute in inducing the antitumor effect;-iii) assess whether short pro-inflammatory stimuli may unleash an effective anti-tumor immune response with consequent tumor regression.

Even though with several limitations, new immunocompetent thyroid tumor models are now being developing, as they represent the next generation tools allowing preclinical studies in the context of a functional immune system [63]. Our initial studies of the *in vivo* impact of COPZ1 silencing showed reduction of tumorigenicity of 8505C cells in nude mice [13]; future studies will certainly include the use of syngeneic immunocompetent mice xenografted with murine thyroid tumor cells, aimed at investigating the effect of COPZ1 depletion on tumor growth, microenvironment and immune response. Since a hallmark of ICD is the induction of tumor-specific immunity *in vivo*, a prophylactic vaccination with COPZ1-depleted cells and the protection from a subsequent tumor challenge should be further assessed.

As for other tumor types, patterns in tumor-associated immune cells within the thyroid cancer microenvironment have been observed, exerting both antitumor and pro-tumor functions [58]. However, low burden of genetic alterations, and therefore antigen scarcity, allow to consider thyroid tumors generally low immunogenic and poor target for immunotherapy [64]. The promotion of ICD certainly may represent an optimal strategy to overcome these limitations. ICD has been poorly explored in thyroid cancer, with the exception of some studies on DAMPs as prognostic markers [65], even if oncolytic virus-based virotherapy, able to induce ICD, has been now considered as strategy to restore immune regulatory properties against tumor cells and to tone down immunosuppressive microenvironment [66]. Our study suggests that COPZ1 depletion, in addition to a direct tempering effect on tumor growth, may have potent immune-stimulatory effects through the establishment of a systemic inflammatory response, thus turning “cold” immunosuppressive thyroid tumors into “hot” inflamed tumors. An intriguing hypothesis for future work is to test whether COPZ1 depletion enhances the efficacy of radiotherapy, chemotherapy or immunotherapy.

Author Disclosure Statement

The authors declare no conflict of interest

Author contributions

Maria Chiara Anania, Angela Greco: conceptualization and design, formal analysis, supervision and writing the original draft; Tiziana Di Marco, Mara Mazzoni, Sonia Pagliardini, Francesca Bianchi, Lucia Sfondrini, Katia Todoerti, Italia Bongarzone, Elisa Maffioli, Gabriella Tedeschi: investigation and validation; Sandra Pellegrini and Antonino Neri: supervision.

Acknowledgments

We thank Dr. Flavio Arienti (Immunohematology and Transfusion Medicine of Fondazione IRCCS Istituto Nazionale dei Tumori, Milan, Italy) for providing buffy coats from healthy donors; Mrs. Gabriella Abolafio (Flow Cytometry Facility of Fondazione IRCCS Istituto Nazionale dei Tumori, Milan, Italy) for technical help; Dr. Valentino Le Noci (Dipartimento di Scienze Biomediche per la Salute, University of Milan, Italy) for help with *in vitro* cytotoxicity assay and Mrs. Silvia Grassi for secretarial assistance. The authors also acknowledge Dr. Patrick Moore for editing the manuscript. This work was supported by Associazione Italiana per la Ricerca sul Cancro [Grant IG 18395, 2017 to A. Greco]. Dr. Francesca Bianchi is a recipient of Fondazione Umberto Veronesi Fellowship. Figures were created with BioRender.com

Name and address of corresponding author

Angela Greco, Fondazione IRCCS Istituto Nazionale dei Tumori, Via G.A. Amadeo, 42, 20133 Milan, Italy. Tel. 0039 02 2390 3222 Fax 0039 02 23903073 e-mail: angela.greco@istitutotumori.mi.it.

References

[1] R.Beck, M.Rawet, F.T.Wieland, and D.Cassel, The COPI system: molecular mechanisms and function. FEBS.Lett. 583 (2009) 2701-2709.

[2] M.Razi, E.Y.Chan, and S.A.Tooze, Early endosomes and endosomal coatomer are required for autophagy. J.Cell Biol 185 (2009) 305-321.

[3] D.Panda, A.Das, P.X.Dinh, S.Subramaniam, D.Nayak, N.J.Barrows, J.L.Pearson, J.Thompson, D.L.Kelly, I.Ladunga, and A.K.Pattnaik, RNAi screening reveals requirement for host cell secretory pathway in infection by diverse families of negative-strand RNA viruses. Proc.Natl.Acad.Sci U.S.A. 108 (2011) 19036-19041.

[4] M.Beller, C.Sztalryd, N.Southall, M.Bell, H.Jackle, D.S.Auld, and B.Oliver, COPI complex is a regulator of lipid homeostasis. PLoS.Biol 6 (2008) e292.

[5] H.Sudo, A.B.Tsuji, A.Sugyo, M.Kohda, C.Sogawa, C.Yoshida, Y.N.Harada, O.Hino, and T.Saga, Knockdown of COPA, identified by loss-of-function screen, induces apoptosis and suppresses tumor growth in mesothelioma mouse model. Genomics. 95 (2010) 210-216.

[6] D.Oliver, H.Ji, P.Liu, A.Gasparian, E.Gardiner, S.Lee, A.Zenteno, L.O.Perinskaya, M.Chen, P.Buckhaults, E.Broude, M.D.Wyatt, H.Valafar, E.Pena, and M.Shtutman, Identification of novel cancer therapeutic targets using a designed and pooled shRNA library screen. Sci Rep. 7 (2017) 43023.

[7] H.S.Kim, S.Mendiratta, J.Kim, C.V.Pecot, J.E.Larsen, I.Zubovych, B.Y.Seo, J.Kim, B.Eskiocak, H.Chung, E.McMillan, S.Wu, B.J.De, K.Komurov, J.E.Toombs, S.Wei, M.Peyton, N.Williams, A.F.Gazdar, B.A.Posner, R.A.Brekken, A.K.Sood, R.J.Deberardinis, M.G.Roth, J.D.Minna, and M.A.White, Systematic identification of molecular subtype-selective vulnerabilities in non-small-cell lung cancer. Cell 155 (2013) 552-566.

[8] X.Pu, J.Wang, W.Li, W.Fan, L.Wang, Y.Mao, S.Yang, S.Liu, J.Xu, Z.Lv, L.Xu, and Y.Shu, COPB2 promotes cell proliferation and tumorigenesis through up-regulating YAP1 expression in lung adenocarcinoma cells. Biomed.Pharmacother. 103 (2018) 373-380.

[9] Z.S.Li, C.H.Liu, Z.Liu, C.L.Zhu, and Q.Huang, Downregulation of COPB2 by RNAi inhibits growth of human cholangiocellular carcinoma cells. Eur Rev.Med.Pharmacol.Sci 22 (2018) 985-992.

[10] C.An, H.Li, X.Zhang, J.Wang, Y.Qiang, X.Ye, Q.Li, Q.Guan, and Y.Zhou, Silencing of COPB2 inhibits the proliferation of gastric cancer cells and induces apoptosis via suppression of the RTK signaling pathway. Int J Oncol. 54 (2019) 1195-1208.

[11] M.Shtutman, M.Baig, E.Levina, G.Hurteau, C.U.Lim, E.Broude, M.Nikiforov, T.T.Harkins, C.S.Carmack, Y.Ding, F.Wieland, R.Buttyan, and I.B.Roninson, Tumor-specific silencing of COPZ2 gene encoding coatomer protein complex subunit zeta 2 renders tumor cells dependent on its paralogous gene COPZ1. Proc.Natl.Acad.Sci U.S.A. 108 (2011) 12449-12454.

[12] M.C.Anania, F.Gasparri, E.Cetti, I.Fraietta, K.Todoerti, C.Miranda, M.Mazzoni, C.Re, R.Colombo, G.Ukmar, S.Camisasca, S.Pagliardini, M.Pierotti, A.Neri, A.Galvani, and

A.Greco, Identification of thyroid tumor cell vulnerabilities through a siRNA-based functional screening. Oncotarget 6 (2015) 34629-34648.

[13] M.C.Anania, E.Cetti, D.Lecis, K.Todoerti, A.Gulino, G.Mauro, Di Marco T., L.Cleris, S.Pagliardini, G.Manenti, B.Belmonte, C.Tripodo, A.Neri, and A.Greco, Targeting COPZ1 non-oncogene addiction counteracts the viability of thyroid tumor cells. Cancer Letters 410 (2017) 201-211.

[14] J.Luo, N.L.Solimini, and S.J.Elledge, Principles of cancer therapy: oncogene and non-oncogene addiction. Cell. 136 (2009) 823-837.

[15] M.E.Cabanillas, D.G.McFadden, and C.Durante, Thyroid cancer. Lancet 388 (2016) 2783-2795.

[16] L.Valerio, L.Pieruzzi, C.Giani, L.Agate, V.Bottici, L.Lorusso, V.Cappagli, L.Puleo, A.Matrone, D.Viola, C.Romei, R.Ciampi, E.Molinaro, and R.Elisei, Targeted Therapy in Thyroid Cancer: State of the Art. Clin Oncol (R.Coll.Radiol.) 29 (2017) 316-324.

[17] X.Shi, R.Liu, F.Basolo, R.Giannini, X.Shen, D.Teng, H.Guan, Z.Shan, W.Teng, T.J.Musholt, K.Al-Kuraya, L.Fugazzola, C.Colombo, E.Kebebew, B.Jarzab, A.Czarniecka, B.Bendlova, V.Sykorova, M.Sobrinho-Simoes, P.Soares, Y.K.Shong, T.Y.Kim, S.Cheng, S.L.Asa, D.Viola, R.Elisei, L.Yip, C.Mian, F.Vianello, Y.Wang, S.Zhao, G.Oler, J.M.Cerutti, E.Puxeddu, S.Qu, Q.Wei, H.Xu, C.J.O'Neill, M.S.Sywak, R.Clifton-Bligh, A.K.Lam, G.Riesco-Eizaguirre, P.Santisteban, H.Yu, G.Tallini, E.H.Holt, V.Vasko, and M.Xing, Differential Clinicopathological Risk and Prognosis of Major Papillary Thyroid Cancer Variants. J Clin Endocrinol.Metab 101 (2016) 264-274.

[18] C.F.Eustatia-Rutten, E.P.Corssmit, N.R.Biermasz, A.M.Pereira, J.A.Romijn, and J.W.Smit, Survival and death causes in differentiated thyroid carcinoma. J Clin Endocrinol.Metab 91 (2006) 313-319.

[19] O.Dohan, l.De, V, V.Paroder, C.Riedel, M.Artani, M.Reed, C.S.Ginter, and N.Carrasco, The sodium/iodide Symporter (NIS): characterization, regulation, and medical significance. Endocr.Rev. 24 (2003) 48-77.

[20] J.M.Gonzalez-Navajas, J.Lee, M.David, and E.Raz, Immunomodulatory functions of type I interferons. Nat Rev.Immunol. 12 (2012) 125-135.

[21] M.Budhwani, R.Mazzieri, and R.Dolcetti, Plasticity of Type I Interferon-Mediated Responses in Cancer Therapy: From Anti-tumor Immunity to Resistance. Front Oncol. 8 (2018) 322.

[22] N.Rufo, A.D.Garg, and P.Agostinis, The Unfolded Protein Response in Immunogenic Cell Death and Cancer Immunotherapy. Trends Cancer 3 (2017) 643-658.

[23] A.D.Garg, A.M.Dudek, and P.Agostinis, Cancer immunogenicity, danger signals, and DAMPs: what, when, and how? Biofactors 39 (2013) 355-367.

[24] L.Zitvogel, L.Galluzzi, O.Kepp, M.J.Smyth, and G.Kroemer, Type I interferons in anticancer immunity. Nat Rev.Immunol. 15 (2015) 405-414.

[25] C.Berges, C.Naujokat, S.Tinapp, H.Wieczorek, A.Hoh, M.Sadeghi, G.Opelz, and V.Daniel, A cell line model for the differentiation of human dendritic cells. Biochem.Biophys.Res Commun. 333 (2005) 896-907.

[26] R.E.Schweppe, J.P.Klopper, C.Korch, U.Pugazhenthi, M.Benezra, J.A.Knauf, J.A.Fagin, L.A.Marlow, J.A.Copland, R.C.Smallridge, and B.R.Haugen, Deoxyribonucleic acid profiling analysis of 40 human thyroid cancer cell lines reveals cross-contamination resulting in cell line redundancy and misidentification. J Clin.Endocrinol.Metab. 93 (2008) 4331-4341.

[27] M.Zhao, D.Sano, C.R.Pickering, S.A.Jasser, Y.C.Henderson, G.L.Clayman, E.M.Sturgis, T.J.Ow, R.Lotan, T.E.Carey, P.G.Sacks, J.R.Grandis, D.Sidransky, N.E.Heldin, and J.N.Myers, Assembly and initial characterization of a panel of 85 genomically validated cell lines from diverse head and neck tumor sites. Clin.Cancer Res. 17 (2011) 7248-7264.

[28] D.Ronchetti, L.Agnelli, A.Pietrelli, K.Todoerti, M.Manzoni, E.Taiana, and A.Neri, A compendium of long non-coding RNAs transcriptional fingerprint in multiple myeloma. Sci Rep. 8 (2018) 6557.

[29] E.E.Schadt, C.Li, B.Ellis, and W.H.Wong, Feature extraction and normalization algorithms for high-density oligonucleotide gene expression array data. J Cell.Biochem.Suppl. Suppl 37 (2001) 120-125.

[30] M.Mattioli, L.Agnelli, S.Fabris, L.Baldini, F.Morabito, S.Bicciato, D.Verdelli, D.Intini, L.Nobili, L.Cro, G.Pruneri, V.Callea, C.Stelitano, A.T.Maiolo, L.Lombardi, and A.Neri, Gene expression profiling of plasma cell dyscrasias reveals molecular patterns associated with distinct IGH translocations in multiple myeloma. Oncogene 24 (2005) 2461-2473.

[31] D.Ronchetti, L.Agnelli, E.Taiana, S.Galletti, M.Manzoni, K.Todoerti, P.Musto, F.Strozzi, and A.Neri, Distinct lncRNA transcriptional fingerprints characterize progressive stages of multiple myeloma. Oncotarget 7 (2016) 14814-14830.

[32] A.Subramanian, P.Tamayo, V.K.Mootha, S.Mukherjee, B.L.Ebert, M.A.Gillette, A.Paulovich, S.L.Pomeroy, T.R.Golub, E.S.Lander, and J.P.Mesirov, Gene set enrichment analysis: a knowledge-based approach for interpreting genome-wide expression profiles. Proc.Natl Acad.Sci U.S.A. 102 (2005) 15545-15550.

[33] E.Taverna, B.M.De, E.Maffioli, C.Corno, E.Ciusani, S.Trivulzio, A.Pinelli, G.Tedeschi, P.Perego, and I.Bongarzone, Alterations of RNA Metabolism by Proteomic Analysis of Breast Cancer Cells Exposed to Marycin: A New Optically Active Porphyrin. Curr.Mol Pharmacol. 12 (2019) 147-159.

[34] J.A.Vizcaino, A.Csordas, N.del-Toro, J.A.Dianes, J.Griss, I.Lavidas, G.Mayer, Y.Perez-Riverol, F.Reisinger, T.Ternent, Q.W.Xu, R.Wang, and H.Hermjakob, 2016 update of the PRIDE database and its related tools. Nucleic Acids Res 44 (2016) D447-D456.

[35] V.Kaimal, E.E.Bardes, S.C.Tabar, A.G.Jegga, and B.J.Aronow, ToppCluster: a multiple gene list feature analyzer for comparative enrichment clustering and network-based dissection of biological systems. Nucleic Acids Res 38 (2010) W96-102.

[36] M.G.Vizioli, M.Sensi, C.Miranda, L.Cleris, F.Formelli, M.C.Anania, M.A.Pierotti, and A.Greco, IGFBP7: an oncosuppressor gene in thyroid carcinogenesis. Oncogene 29 (2010) 3835-3844.

[37] V.Le Noci, S.Guglielmetti, S.Arioli, C.Camisaschi, F.Bianchi, M.Sommariva, C.Storti, T.Triulzi, C.Castelli, A.Balsari, E.Tagliabue, and L.Sfondrini, Modulation of Pulmonary Microbiota by Antibiotic or Probiotic Aerosol Therapy: A Strategy to Promote Immunosurveillance against Lung Metastases. Cell Rep. 24 (2018) 3528-3538.

[38] M.Musella, G.Manic, M.R.De, I.Vitale, and A.Sistigu, Type-I-interferons in infection and cancer: Unanticipated dynamics with therapeutic implications. Oncoimmunology 6 (2017) e1314424.

[39] E.N.Fish and L.C.Platanias, Interferon receptor signaling in malignancy: a network of cellular pathways defining biological outcomes. Mol Cancer Res 12 (2014) 1691-1703.

[40] A.Sistigu, T.Yamazaki, E.Vacchelli, K.Chaba, D.P.Enot, J.Adam, I.Vitale, A.Goubar, E.E.Baracco, C.Remedios, L.Fend, D.Hannani, L.Aymeric, Y.Ma, M.Niso-Santano, O.Kepp, J.L.Schultze, T.Tuting, F.Belardelli, L.Bracci, S.La, V, G.Zicchedu, P.Sestili, F.Urbani, M.Delorenzi, M.Lacroix-Triki, V.Quidville, R.Conforti, J.P.Spano, L.Pusztai, V.Poirier-Colame, S.Delaloge, F.Penault-Llorca, S.Ladoire, L.Arnould, J.Cyrta, M.C.Dessoliers, A.Eggermont, M.E.Bianchi, M.Pittet, C.Engblom, C.Pfirschke, X.Preville, G.Uze, R.D.Schreiber, M.T.Chow, M.J.Smyth, E.Proietti, F.Andre, G.Kroemer, and L.Zitvogel, Cancer cell-autonomous contribution of type I interferon signaling to the efficacy of chemotherapy. Nat Med. 20 (2014) 1301-1309.

[41] A.D.Garg and P.Agostinis, Cell death and immunity in cancer: From danger signals to mimicry of pathogen defense responses. Immunol.Rev. 280 (2017) 126-148.

[42] A.D.Garg, L.Galluzzi, L.Apetoh, T.Baert, R.B.Birge, J.M.Bravo-San Pedro, K.Breckpot, D.Brough, R.Chaurio, M.Cirone, A.Coosemans, P.G.Coulie, R.D.De, L.Dini, W.P.de, A.M.Dudek-Peric, A.Faggioni, J.Fucikova, U.S.Gaipl, J.Golab, M.L.Gougeon, M.R.Hamblin, A.Hemminki, M.Herrmann, J.W.Hodge, O.Kepp, G.Kroemer, D.V.Krysko, W.G.Land, F.Madeo, A.A.Manfredi, S.R.Mattarollo, C.Maueroder, N.Merendino, G.Multhoff, T.Pabst, J.E.Ricci, C.Riganti, E.Romano, N.Rufo, M.J.Smyth, J.Sonnemann, R.Spisek, J.Stagg, E.Vacchelli, P.Vandenabeele, L.Vandenberk, B.J.Van den Eynde, G.S.Van, F.Velotti, L.Zitvogel, and P.Agostinis, Molecular and Translational Classifications of DAMPs in Immunogenic Cell Death. Front Immunol. 6 (2015) 588.

[43] G.Kroemer, L.Galluzzi, O.Kepp, and L.Zitvogel, Immunogenic cell death in cancer therapy. Annu.Rev.Immunol. 31 (2013) 51-72.

[44] S.Volpi, J.Tsui, M.Mariani, C.Pastorino, R.Caorsi, O.Sacco, A.Ravelli, A.K.Shum, M.Gattorno, and P.Picco, Type I interferon pathway activation in COPA syndrome. Clin.Immunol. 187 (2018) 33-36.

[45] L.B.Watkin, B.Jessen, W.Wiszniewski, T.J.Vece, M.Jan, Y.Sha, M.Thamsen, R.L.Santos-Cortez, K.Lee, T.Gambin, L.R.Forbes, C.S.Law, A.Stray-Pedersen, M.H.Cheng, E.M.Mace, M.S.Anderson, D.Liu, L.F.Tang, S.K.Nicholas, K.Nahmod, G.Makedonas, D.L.Canter, P.Y.Kwok, J.Hicks, K.D.Jones, S.Penney, S.N.Jhangiani, M.D.Rosenblum, S.D.Dell, M.R.Waterfield, F.R.Papa, D.M.Muzny, N.Zaitlen, S.M.Leal, C.Gonzaga-Jauregui, E.Boerwinkle, N.T.Eissa, R.A.Gibbs, J.R.Lupski, J.S.Orange, and A.K.Shum, COPA

mutations impair ER-Golgi transport and cause hereditary autoimmune-mediated lung disease and arthritis. Nat.Genet. 47 (2015) 654-660.

[46] T.J.Vece, L.B.Watkin, S.Nicholas, D.Canter, M.C.Braun, R.P.Guillerman, K.W.Eldin, G.Bertolet, S.McKinley, G.M.de, L.Forbes, I.Chinn, and J.S.Orange, Copa Syndrome: a Novel Autosomal Dominant Immune Dysregulatory Disease. J Clin.Immunol. 36 (2016) 377-387.

[47] F.Bianchi, S.Pretto, E.Tagliabue, A.Balsari, and L.Sfondrini, Exploiting poly(I:C) to induce cancer cell apoptosis. Cancer Biol Ther. 18 (2017) 747-756.

[48] R.F.V.Medrano, A.Hunger, S.A.Mendonca, J.A.M.Barbuto, and B.E.Strauss, Immunomodulatory and antitumor effects of type I interferons and their application in cancer therapy. Oncotarget 8 (2017) 71249-71284.

[49] T.Li and Z.J.Chen, The cGAS-cGAMP-STING pathway connects DNA damage to inflammation, senescence, and cancer. J Exp Med 215 (2018) 1287-1299.

[50] K.P.Kotredes and A.M.Gamero, Interferons as inducers of apoptosis in malignant cells. J Interferon Cytokine Res 33 (2013) 162-170.

[51] W.I.Lencer, H.DeLuca, M.J.Grey, and J.A.Cho, Innate immunity at mucosal surfaces: the IRE1-RIDD-RIG-I pathway. Trends Immunol. 36 (2015) 401-409.

[52] C.Uggenti, A.Lepelley, and Y.J.Crow, Self-Awareness: Nucleic Acid-Driven Inflammation and the Type I Interferonopathies. Annu.Rev.Immunol. 37 (2019) 247-267.

[53] J.J.Bernard, C.Cowing-Zitron, T.Nakatsuji, B.Muehleisen, J.Muto, A.W.Borkowski, L.Martinez, E.L.Greidinger, B.D.Yu, and R.L.Gallo, Ultraviolet radiation damages self noncoding RNA and is detected by TLR3. Nat Med. 18 (2012) 1286-1290.

[54] N.Dicks, K.Gutierrez, M.Michalak, V.Bordignon, and L.B.Agellon, Endoplasmic reticulum stress, genome damage, and cancer. Front Oncol. 5 (2015) 11.

[55] R.D.Paulsen, D.V.Soni, R.Wollman, A.T.Hahn, M.C.Yee, A.Guan, J.A.Hesley, S.C.Miller, E.F.Cromwell, D.E.Solow-Cordero, T.Meyer, and K.A.Cimprich, A genome-wide siRNA screen reveals diverse cellular processes and pathways that mediate genome stability. Mol Cell 35 (2009) 228-239.

[56] S.Muralidharan and P.Mandrekar, Cellular stress response and innate immune signaling: integrating pathways in host defense and inflammation. J Leukoc.Biol 94 (2013) 1167-1184.

[57] A.Showalter, A.Limaye, J.L.Oyer, R.Igarashi, C.Kittipatarin, A.J.Copik, and A.R.Khaled, Cytokines in immunogenic cell death: Applications for cancer immunotherapy. Cytokine 97 (2017) 123-132.

[58] S.M.Ferrari, P.Fallahi, M.R.Galdiero, I.Ruffilli, G.Elia, F.Ragusa, S.R.Paparo, A.Patrizio, V.Mazzi, G.Varricchi, G.Marone, and A.Antonelli, Immune and Inflammatory Cells in Thyroid Cancer Microenvironment. Int J Mol Sci 20 (2019).

[59] G.Varricchi, S.Loffredo, G.Marone, L.Modestino, P.Fallahi, S.M.Ferrari, P.A.de, A.Antonelli, and M.R.Galdiero, The Immune Landscape of Thyroid Cancer in the Context of Immune Checkpoint Inhibition. Int J Mol Sci 20 (2019).

[60] F.Coperchini, L.Croce, M.Marino, L.Chiovato, and M.Rotondi, Role of chemokine receptors in thyroid cancer and immunotherapy. Endocr.Relat Cancer2019).

[61] A.J.Minn, Interferons and the Immunogenic Effects of Cancer Therapy. Trends Immunol. 36 (2015) 725-737.

[62] E.Tomasello, E.Pollet, T.P.Vu Manh, G.Uze, and M.Dalod, Harnessing Mechanistic Knowledge on Beneficial Versus Deleterious IFN-I Effects to Design Innovative Immunotherapies Targeting Cytokine Activity to Specific Cell Types. Front Immunol. 5 (2014) 526.

[63] P.Vanden Borre, D.G.McFadden, V.Gunda, P.M.Sadow, S.Varmeh, M.Bernasconi, T.Jacks, and S.Parangi, The next generation of orthotopic thyroid cancer models: immunocompetent orthotopic mouse models of BRAF V600E-positive papillary and anaplastic thyroid carcinoma. Thyroid 24 (2014) 705-714.

[64] L.M.Colli, M.J.Machiela, T.A.Myers, L.Jessop, K.Yu, and S.J.Chanock, Burden of Nonsynonymous Mutations among TCGA Cancers and Candidate Immune Checkpoint Inhibitor Responses. Cancer Res 76 (2016) 3767-3772.

[65] R.C.Mould, J.P.van Vloten, A.W.K.AuYeung, K.Karimi, and B.W.Bridle, Immune responses in the thyroid cancer microenvironment: making immunotherapy a possible mission. Endocr.Relat Cancer 24 (2017) T311-T329.

[66] A.M.Malfitano, S.D.Somma, N.Prevete, and G.Portella, Virotherapy as a Potential Therapeutic Approach for the Treatment of Aggressive Thyroid Cancer. Cancers (Basel) 11 (2019).

Table I: Functional annotation clustering on 99 differentially expressed genes in COPZ1-depleted TPC-1 cells in comparison to siNT control cells.

Annotation Cluster n°	ES	GO Annotation Term	%	FDR
1	9.96	**GO:0006986~ response to unfolded protein**	14.29	7.75E-09
2	6.71	**GO:0042175~ nuclear outer membrane-endoplasmic reticulum membrane network**	24.49	1.94E-05
3	6.09	**GO:0048193~ Golgi vesicle transport**	14.29	1.61E-05
4	5.53	**GO:0001817~ regulation of cytokine production**	15.31	2.49E-03
5	5.52	**GO:0015031~ protein transport**	28.57	6.45E-04
6	4.81	**GO:0034613~ cellular protein localization**	23.47	2.58E-02
7	3.00	**GO:0030120~ vesicle coat**	5.10	2.49E-01
8	2.73	**GO:0009607~ response to biotic stimulus**	14.29	9.09E-01
9	2.70	**GO:0048208~ COPII vesicle coating**	5.10	4.89E-01
10	2.68	**GO:0032653~ regulation of interleukin-10 production**	4.08	2.82
11	2.66	**GO:0071216~ cellular response to biotic stimulus**	9.18	5.94E-04
12	2.33	**GO:1902235~ regulation of endoplasmic reticulum stress-induced intrinsic apoptotic signaling pathway**	4.08	1.04
13	2.32	**GO:0002700~ regulation of production of molecular mediator of immune response**	5.10	3.97
14	2.23	**GO:2001234~ negative regulation of apoptotic signaling pathway**	8.16	1.88E-01
15	2.11	**GO:0002697~ regulation of immune effector process**	8.16	2.55
16	2.10	**GO:0030662~ coated vesicle membrane**	7.14	2.26E-01
17	2.02	**GO:0061043~ regulation of vascular wound healing**	3.06	4.62E-01

Representative GO terms are reported for the 17 significant clusters out of 114 total clusters (Enrichment Score, ES >2, p-value < 0.01). The percentage of significant genes in GO-term and false discovery rate (FDR) are also indicated for each annotation cluster.

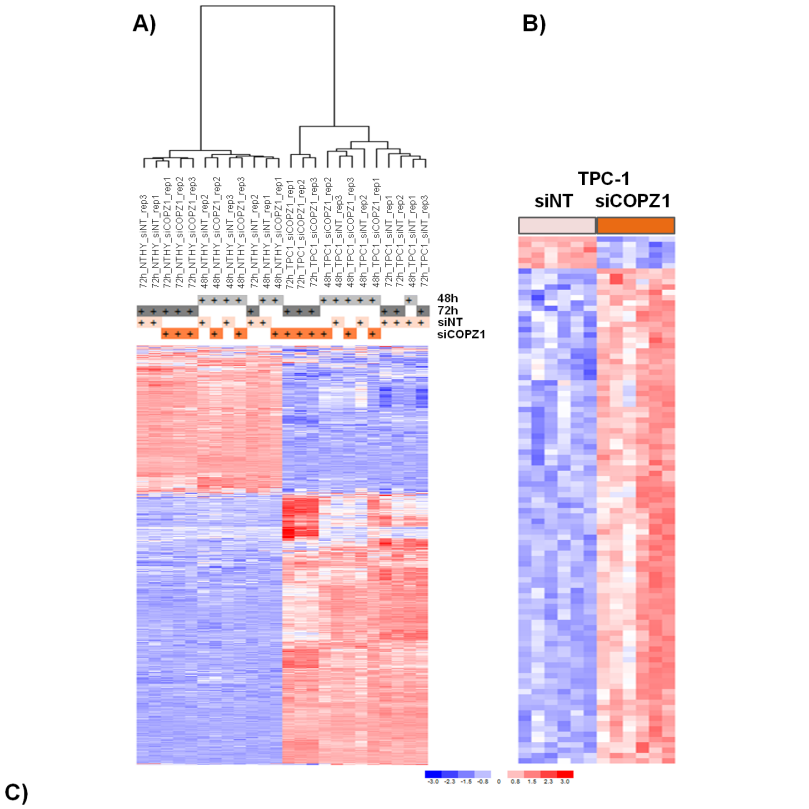
A)
B)
TPC-1
siNT
siCOPZ1
72h_NTHY_siNT_rep3
72h_NTHY_siNT_rep1
72h_NTHY_siCOPZ1_rep1
72h_NTHY_siCOPZ1_rep2
72h_NTHY_siCOPZ1_rep3
48h_NTHY_siNT_rep2
48h_NTHY_siCOPZ1_rep2
48h_NTHY_siCOPZ1_rep3
72h_NTHY_siNT_rep2
48h_NTHY_siNT_rep1
48h_NTHY_siCOPZ1_rep1
72h_TPC1_siCOPZ1_rep1
72h_TPC1_siCOPZ1_rep2
72h_TPC1_siCOPZ1_rep3
48h_TPC1_siNT_rep3
48h_TPC1_siCOPZ1_rep2
48h_TPC1_siNT_rep2
48h_TPC1_siCOPZ1_rep1
72h_TPC1_siNT_rep1
72h_TPC1_siNT_rep2
48h_TPC1_siNT_rep1
72h_TPC1_siNT_rep3
48h
72h
siNT
siCOPZ1

C)

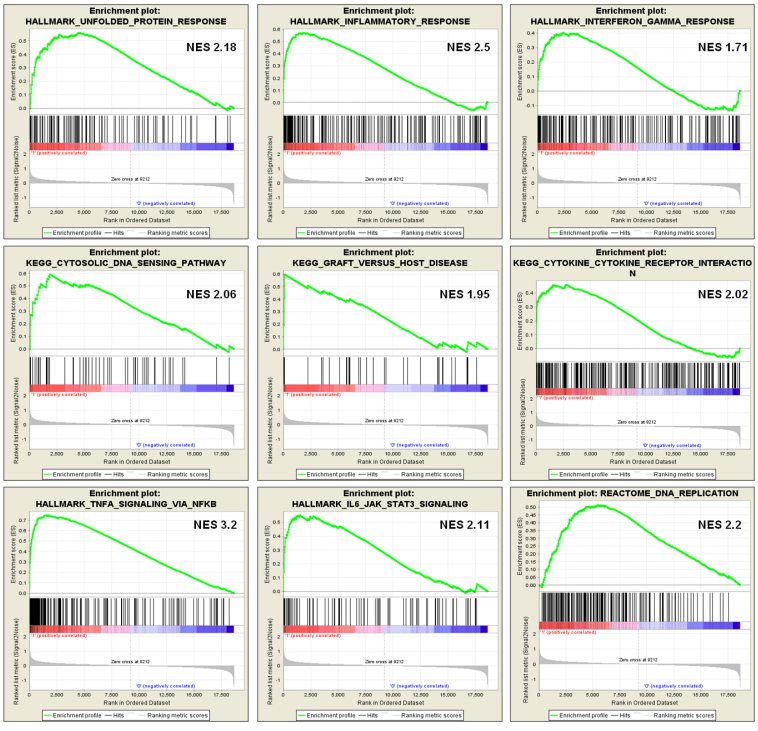
Enrichment plot:
HALLMARK_UNFOLDED_PROTEIN_RESPONSE
NES 2.18
Enrichment plot:
HALLMARK_INFLAMMATORY_RESPONSE
NES 2.5
Enrichment plot:
HALLMARK_INTERFERON_GAMMA_RESPONSE
NES 1.71
Enrichment plot:
KEGG_CYTOSOLIC_DNA_SENSING_PATHWAY
NES 2.06
Enrichment plot:
KEGG_GRAFT_VERSUS_HOST_DISEASE
NES 1.95
Enrichment plot:
KEGG_CYTOKINE_CYTOKINE_RECEPTOR_INTERACTIO
N
NES 2.02
Enrichment plot:
HALLMARK_TNFA_SIGNALING_VIA_NFKB
NES 3.2
Enrichment plot:
HALLMARK_IL6_JAK_STAT3_SIGNALING
NES 2.11
Enrichment plot: REACTOME_DNA_REPLICATION
NES 2.2

A)

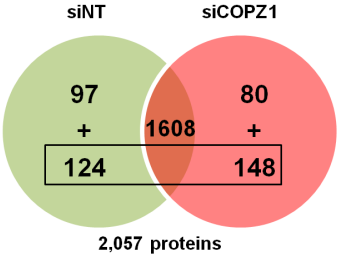

B)

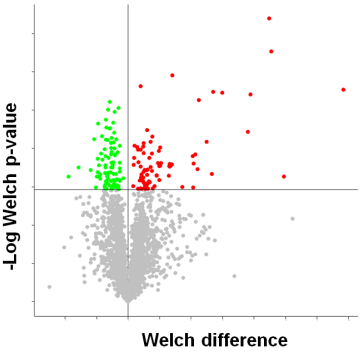

Top up modulated

H2AX
APP
HIST1H4A
VIM
ICAM1
LAMB3
HIST1H2AB
ISG15
SPARC
CLU
MAVS

Top down modulated

AP2M1
TYMS
KIAA0664
COPB2
DCDC2
PDLIM7
Nup155
GPI
MCM6

C)

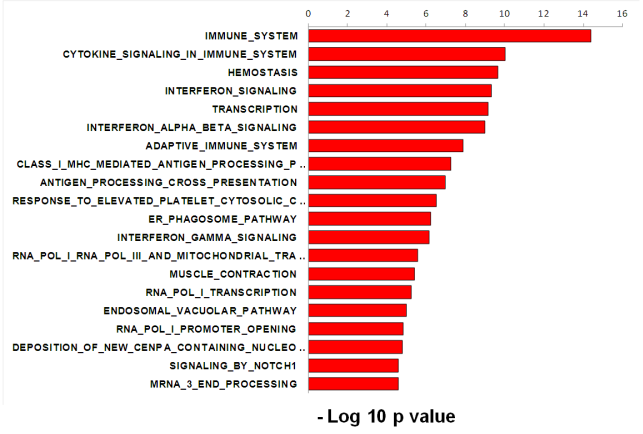

D)

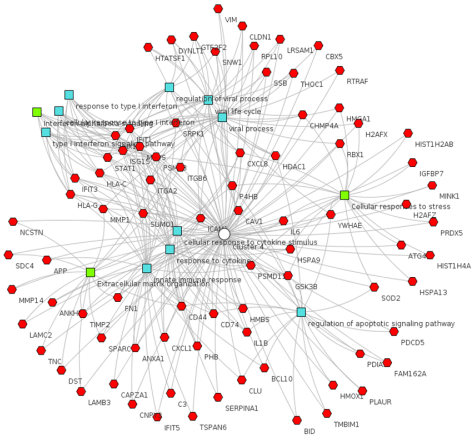

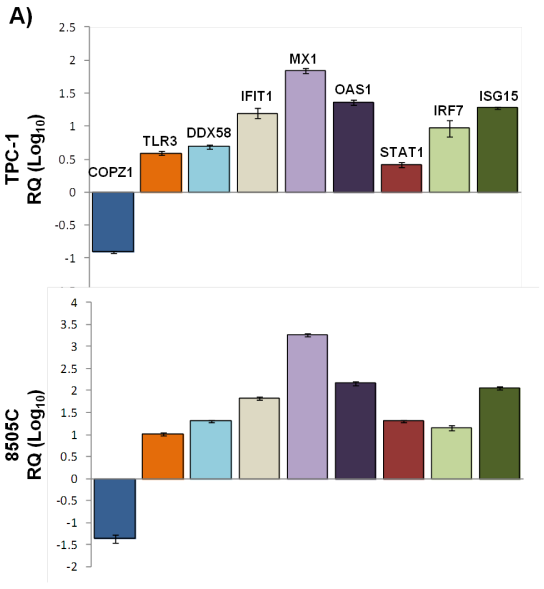

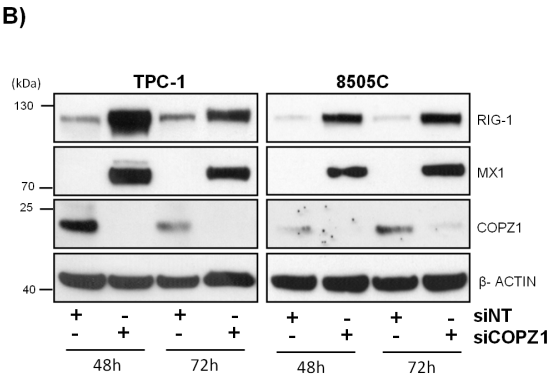

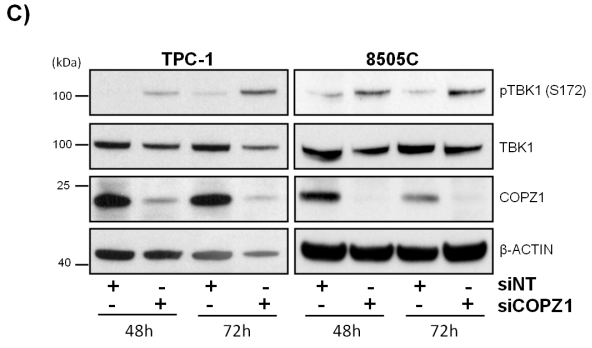

D)

	TPC-1		8505C	
AKT1	0.08	0.01	0.36	0.04
ATF6	0.32	0.12	0.26	0.23
ATM	0.36	0.06	0.27	0.28
CASP1	0.63	0.00	0.74	0.82
CASP8	0.42	0.04	0.15	0.13
CD274	0.86	0.52	0.22	0.03
CDKN1A	0.81	0.47	0.71	0.57
CDKN2A	-0.29	-0.23	0.18	-0.12
COPZ1	-1.00	-0.60	-1.33	-1.30
ERN1	0.94	0.60	0.88	0.95
HLA-DRB1	1.07	0.29	ND	-0.31
HMGB1	-0.03	-0.19	-0.39	-0.26
IFIH1	1.22	0.68	1.62	1.11
IFIT1	1.51	0.56	1.31	0.98
IFIT2	0.89	0.30	0.88	0.29
IFNA1	0.05	-0.28	-0.29	0.07
IFNAR1	0.38	0.18	0.12	0.20
IFNB1	1.48	1.21	1.32	1.19
IFNG	ND	ND	ND	ND
IFNGR1	0.43	0.13	0.12	0.22
IRF1	0.41	0.40	0.32	0.10
IRF3	0.12	0.04	0.09	0.17
IRF7	1.21	0.61	1.24	0.92
IRF9	0.63	0.23	1.02	0.73
ISG15	1.41	0.84	2.01	1.74
MB21D1	0.30	0.17	-0.54	-0.09
MX1	2.23	1.32	3.32	2.41
MX2	3.30	2.03	3.64	2.71
NFKB1	0.69	0.45	0.44	0.34
NOD1	0.19	-0.11	0.44	0.08
OAS1	1.65	0.90	1.90	1.22
OAS3	1.22	0.84	1.58	1.12
OASL	1.76	1.13	2.76	1.59
PDCD1	ND	ND	1.03	0.68
STAT1	0.72	0.26	1.41	1.08
STAT2	0.60	0.09	1.00	0.54
STAT3	0.06	0.05	0.25	-0.05
TLR2	0.76	0.28	0.54	0.22
TLR4	0.10	-0.26	0.27	0.03
TMEM173	0.33	0.08	0.36	0.10
	48h	72h	48h	72h

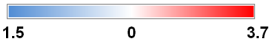

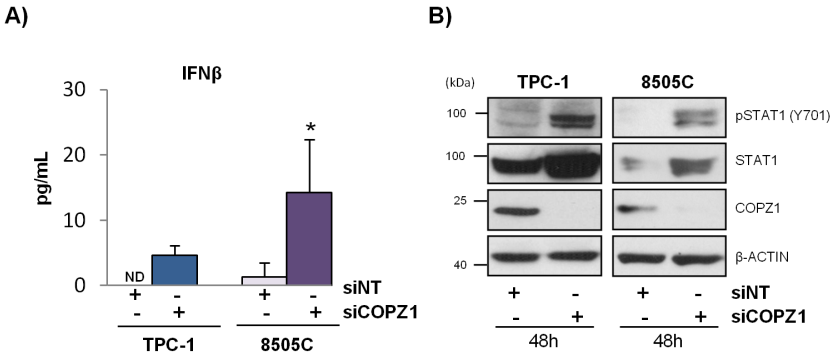

C)

	IDO1	PTGS2	PTX3	CCL17	CCL18	CCL2	CCL20	CCL3	CCL5	CCL7	CCR1	CSF1	CSF2	CXCL1	CXCL10	CXCL12	CXCL8	CXCR2	
48h	2,08	2,06	1,55	ND	ND	0,92	3,15	1,46	2,68	1,17	ND	-0,05	2,31	1,49	2,98	0,00	2,98	ND	TPC-1
72h	1,47	2,64	0,71	ND	ND	0,40	2,93	1,85	1,65	1,28	-0,68	-0,31	1,31	0,87	1,74	0,00	1,71	ND	
48h	1,22	0,72	0,34	ND	ND	-0,43	1,52	1,01	2,95	ND	1,30	0,43	0,47	0,27	2,53	-0,57	0,49	ND	8505C
72h	0,42	0,82	0,59	ND	ND	-0,69	0,89	0,63	1,58	-0,20	0,54	0,24	0,85	0,19	1,66	-1,27	0,71	ND	

	CXCR3	CXCR4	IL10	IL12A	IL12B	IL18	IL1A	IL1B	IL1R1	IL2	IL4	IL6	SPARC	SPP1	TGFB1	TNF	TNFRSF1B	VEGFA	
48h	-1,25	0,60	0,00	0,67	-0,66	-0,66	2,41	2,29	0,53	ND	ND	2,06	-0,15	-0,60	-0,20	1,47	2,07	0,53	TPC-1
72h	-0,30	0,65	-0,29	-0,08	-0,15	0,00	1,80	1,39	0,37	ND	ND	1,30	-0,49	-0,82	-0,11	0,69	1,97	0,41	
48h	ND	0,19	ND	0,43	ND	0,26	1,01	0,55	-0,14	ND	ND	1,04	0,13	-0,28	0,21	0,63	0,54	0,33	8505C
72h	ND	0,31	ND	0,49	ND	0,27	1,03	0,79	-0,16	-0,94	ND	0,79	-0,30	-0,81	0,02	0,17	0,21	0,15	

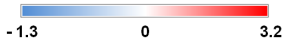

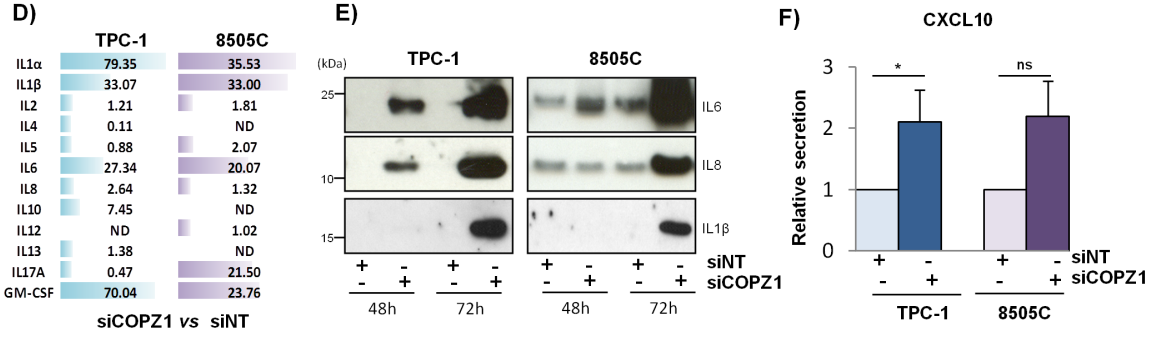

A)

		siNT		siCOPZ1	
		% live cells	% CRT	% live cells	% CRT
TPC-1	48h	99.00	0.11	63.00	6.13
	72h	97.3	0.54	7.76	16.4
	96h	95.8	0.23	6.64	29.4
8505C	48h	96.7	0.46	94.4	0.56
	72h	96.7	0.37	67.6	9.95
	96h	94.8	0.73	28.8	46.1

B)

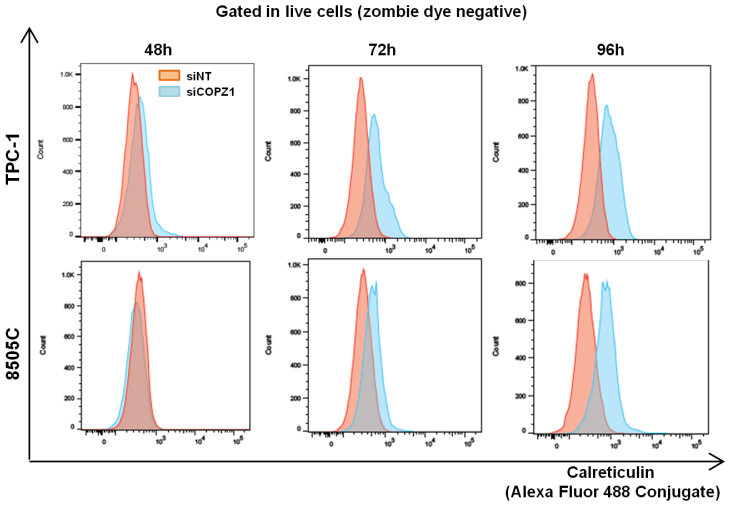

C)

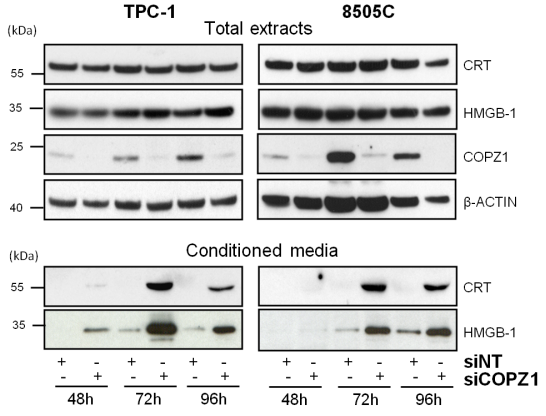

D)

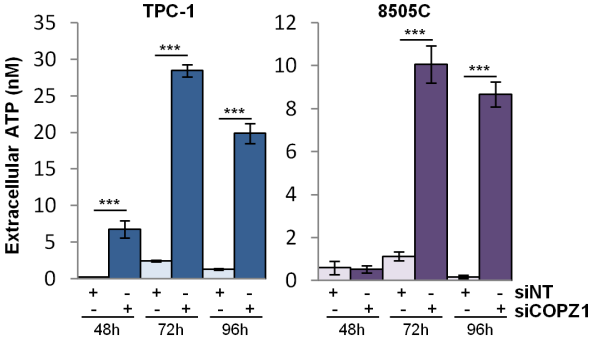

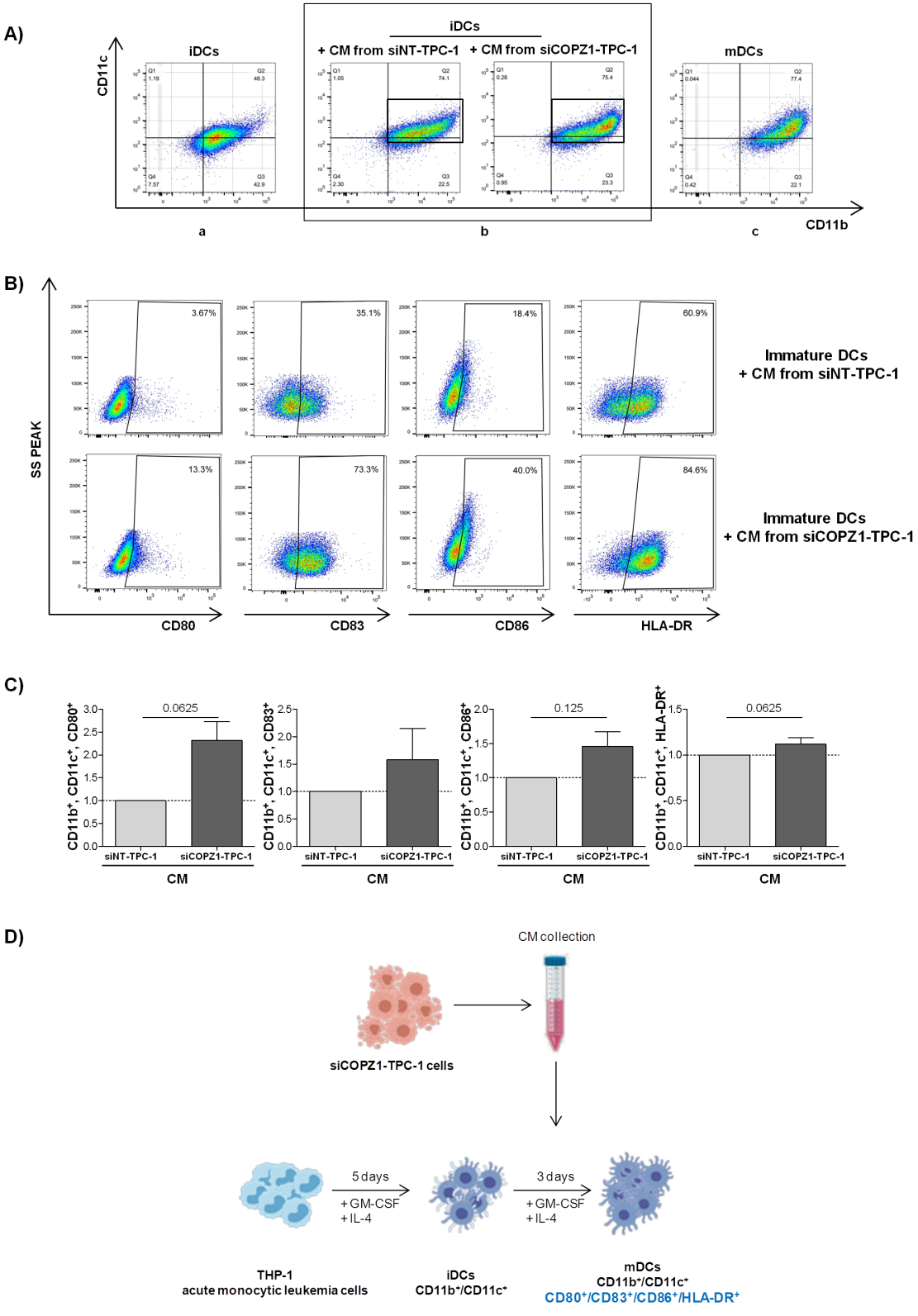
A)
iDCs
iDCs
+ CM from siNT-TPC-1
+ CM from siCOPZ1-TPC-1
mDCs
CD11c
CD11b
a
b
c
B)
SS PEAK
3.67%
35.1%
18.4%
60.9%
13.3%
73.3%
40.0%
84.6%
Immature DCs
+ CM from siNT-TPC-1
Immature DCs
+ CM from siCOPZ1-TPC-1
CD80
CD83
CD86
HLA-DR
C)
CD11b+, CD11c+, CD80+
CD11b+, CD11c+, CD83+
CD11b+, CD11c+, CD86+
CD11b+, CD11c+, HLA-DR+
0.0625
0.125
0.0625
siNT-TPC-1
siCOPZ1-TPC-1
CM
D)
CM collection
siCOPZ1-TPC-1 cells
5 days
+ GM-CSF
+ IL-4
3 days
+ GM-CSF
+ IL-4
THP-1
acute monocytic leukemia cells
iDCs
CD11b+/CD11c+
mDCs
CD11b+/CD11c+
CD80+/CD83+/CD86+/HLA-DR+

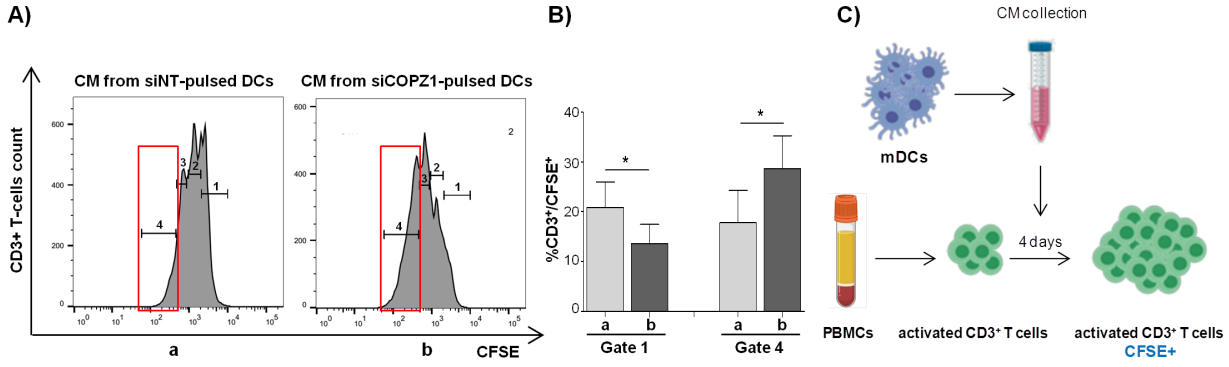
A)
CM from siNT-pulsed DCs
CM from siCOPZ1-pulsed DCs
CD3+ T-cells count
CFSE
a
b
B)
%CD3+/CFSE+
Gate 1
Gate 4
C)
CM collection
mDCs
4 days
PBMCs
activated CD3+ T cells
activated CD3+ T cells
CFSE+

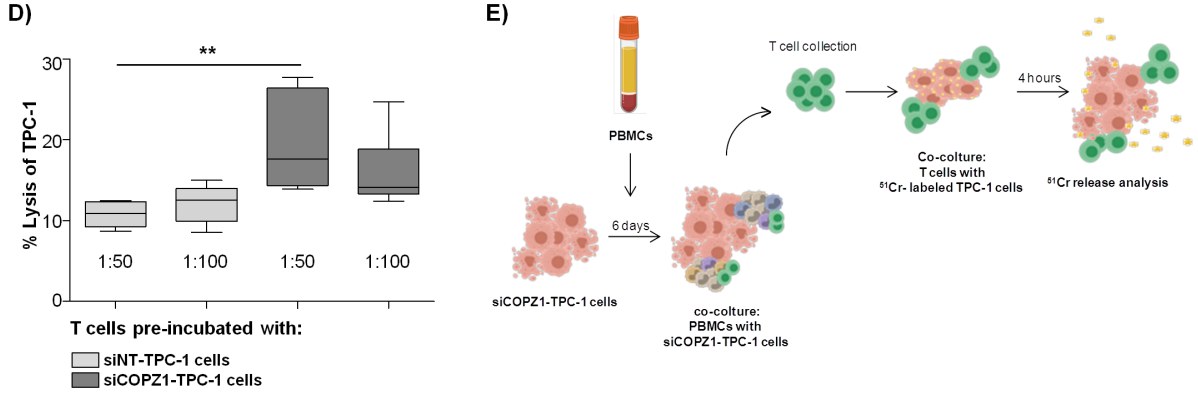
D)
% Lysis of TPC-1
1:50
1:100
1:50
1:100
T cells pre-incubated with:
siNT-TPC-1 cells
siCOPZ1-TPC-1 cells
E)
PBMCs
6 days
siCOPZ1-TPC-1 cells
co-colture:
PBMCs with
siCOPZ1-TPC-1 cells
T cell collection
Co-colture:
T cells with
51Cr- labeled TPC-1 cells
4 hours
51Cr release analysis

Figure legends

Fig. 1: Gene expression profiling of COPZ1-depleted TPC-1 cells. (A) Hierarchical clustering of TPC-1 and NThy-ori 1-3 replicates (48 h, 72 h after siRNA transfection) on the 857 most variable genes across the entire dataset. **(B)** Heatmap of 99 significant differentially expressed genes in TPC-1 replicates after COPZ1 silencing at both 48 h and 72 h siRNA transfection. The color changes in each row represent the gene expression relative to the mean across the samples. **c** Enrichment plots of selected gene sets that were significantly upregulated in TPC-1 cells at 72 h after siRNA transfection. The enrichment score (ES) plotted as a function of the position within the ranked list of array genes is shown as a green line. At the bottom of the plot, the ranked list metric shown in gray illustrates the correlation of gene expression values with phenotypes. Signal intensities are illustrated by varying shades of red (up-regulation) and blue (down-regulation). The normalized enrichment score (NES) is reported for each plot. siNT: Non-Targeting siRNAs; siCOPZ1: siRNAs targeting COPZ1.

Fig. 2: Proteome analysis of COPZ1-depleted TPC-1 cells. (A) Venn diagram displays up-regulated and down-regulated proteins in siCOPZ1 *vs* siNT control cells considering the total number of identified proteins. Differentially expressed proteins were determined using Welch's *t* test (p value < 0.05). A total of 177 proteins (80 up and 97 down) were differentially expressed with a p value < 0.05 in siCOPZ1 cells *vs* siNT control cells; 148 and 124 proteins were exclusively found in control or siCOPZ1 cells, respectively. **(B)** Volcano plot showing the results of differentially expressed proteins based on fold change *vs* t-test probability (Welch difference). Each protein is represented as a dot and is mapped according to its fold change on the ordinate axis (y), with the p-value by t-test on the abscissa (x). The red and green dots indicate up-regulated and down-regulated proteins, respectively. Grey dots do not meet the fold and p-value criteria. The top significantly up-down-regulated proteins are listed. **(C)** Pathway information from the Reactome Database using GSEA website for enrichment analysis; the bar plot shows the significant top

enrichment scores (−log p value). **(D)** Networks generated using the lists of up-modulated proteins in siCOPZ1 cells *vs* siNT control. This functional association analysis was performed by ToppCluster based on pathway networks showing enriched terms from Gene Ontology and pathways; red dot: differentially expressed proteins; green square: pathways; light blue square: biological process.

Fig. 3: COPZ1 depletion in TPC-1 and 8505C cells is associated with the type I interferon response. (A) Real-time PCR analysis of gene expression at 48 h after siRNA transfection. Results are presented as relative quantity (RQ Log_{10}) normalized for HPRT-1 housekeeping gene expression. Data are normalized as ratio to the corresponding control, considered siNT =0 as baseline; data represent the mean ± SD of three independent experiments. **(B,C)** western blot analysis for expression of COPZ1, RIG-1, MX1, pTBK1(S172), and TBK1 proteins at the indicated time points after siRNA transfection; β-actin was used for normalization of gel loading. **(D)** qRT-PCR analysis with a customized TaqMan Low Density Array of 40 genes related to the interferon pathway at 48 h and 72 h after siRNA transfection. Values are presented as in A and represent the mean of two independent experiments. ND: not detected. siNT: Non-Targeting siRNAs; siCOPZ1: siRNAs targeting COPZ1.

Fig. 4: COPZ1 depletion in TPC-1 and 8505C cells is associated with type I interferon-induced inflammation. (A) The histograms show the level of IFN-β secretion detected by ELISA in CM collected at 72 h after siRNA transfection; samples were analyzed in duplicate in three independent experiments; the asterisk indicates significant differences by paired Student's *t* test (*$p<0.05$); ND: not detected. **(B)** western blot analysis for the expression of pSTAT1 (Y701), STAT1, and COPZ1 proteins at the indicated time points after siRNA transfection; β-actin was used for normalization of gel loading. **(C)** qRT-PCR analysis with a customized TaqMan Low Density Array of 36 genes related to immune-inflammatory pathways at 48 h and 72 h after siRNA

transfection. Results are presented as relative quantity (RQ Log_{10}) normalized for HPRT-1 housekeeping gene expression. Data are normalized as ratio to the corresponding control, considering siNT=0 as baseline and represent the mean of two independent experiments; ND: not detected. **(D)** CM as in A were analyzed by a multianalyte ELISA array for secretion of a panel of cytokines; results are expressed as fold change relative to the siNT controls; ND: not detected. **E)** western blot analysis for expression of IL6, IL8, and IL1β in CM produced as in A; Ponceau S staining of membranes for checking protein loading is provided in Fig. S5. **F)** The histograms show the relative secretion of CXCL10 detected by ELISA in CM collected at 72 h after siRNA transfection; samples were analyzed in duplicate in three independent experiments (siNT =1). *p < 0.05 by paired Student's *t* test; ns: not significant p = 0.059.

Fig. 5: Detection of DAMPs in COPZ1-depleted cells. TPC-1 and 8505C cells, at different time points after siRNA transfection, were analyzed by: **(A)** Flow cytometry analysis of surface calreticulin (CRT); in the table percentage of live cells, assessed with zombie dye, and calreticulin-expressing cells are reported; a representative analysis of three independent experiments is shown; **(B)** Representative overlay histogram plots showing the mean fluorescence intensity of viable cells expressing ecto-CRT; **(C)** western blot for the expression of calreticulin and HMGB1 proteins in total extracts (top panel) and CM (bottom panel); Ponceau S staining of membranes for checking protein loading is provided in Fig. S5. **(D)** extracellular ATP quantification in CM; samples were analyzed in triplicate; a representative analysis of three independent experiments is shown; asterisks indicate significant differences by the unpaired Student's *t* test (***p<0.001).

Fig. 6: COPZ1-induced cell death promotes dendritic cell maturation. (A) immature DCs (iDCs) untreated (a) or cultured for 3 days with CM from COPZ1-silenced (or siNT- as a control) TPC-1 cells (b), and iDCs induced to maturation with specific stimulatory factors (positive control) (c) were evaluated by flow cytometry for the expression of CD11c and CD11b markers. **(B)**

representative dot plots of $CD11b^+CD11c^+$ iDCs cultured with CM from COPZ1-silenced (or siNT) TPC-1 cells (b) assessed by flow cytometry for the expression of CD80, CD83, CD86, and HLA-DR markers. **(C)** histograms illustrate the relative fold increase expression of CD80, CD83, CD86, and HLA-DR markers, detected by flow cytometry as in (B), in iDCs cultured with COPZ-1-silenced TPC-1 vs. siNT from four independent experiments; significance difference by non parametric Wilcoxon matched pairs test. **(D)** Graphical representation of the experimental procedure; figure was created with BioRender.

Fig.7: COPZ1-induced cell death promotes T cell proliferation and cytotoxic activity. (A) Representative dot plots of CFSE-labelled $CD3^+$ T cells, stimulated with anti-CD3/CD28 dynabeads, cultured for 4 days with CM derived from pulsed siNT (a) and siCOPZ1 (b) DCs TPC-1 and assessed for proliferation. **(B)** histograms illustrate the percentage (±SD) of $CD3^+$ T cells evaluated in gate 1 and gate 4 of proliferation process from five independent experiments; *$p < 0.5$ by unpaired Student's *t* test. **(D)** Percentage of lysis of ^{51}Cr-labeled TPC-1 target cells after 4 h of culture in the presence of T-cells, pre-incubated for 6 days with siCOPZ1-TPC-1 cells or siNT-TPC-1 cells as a control (target:effector ratio 1:50 and 1:100). Box and whiskers: min to max represent data pooled from 2 independent experiments performed in triplicate. asterisks indicate significant differences by the unpaired Student's *t* test (**$p<0.01$)**.** In **(C)** and **(E)** Graphical representation of the experimental procedures are reported; figures were created with BioRender.

Highlights

- COPZ1 represents a non-oncogene addiction for thyroid cancer
- COPZ1 silencing stimulates type I IFN response and inflammation
- COPZ1 silencing induces immunogenic cell death, dendritic and T cell activation
- COPZ1 depletion prompts an anti-tumor immune response
- COPZ1 targeting represents a new therapeutic strategy for advanced thyroid cancer

FONDAZIONE IRCCS
ISTITUTO NAZIONALE
DEI TUMORI
20133 Milano - via Venezian, 1 - tel. 02.2390.1 - codice fiscale 80018230153 - partita i.v.a. 04376350155

Dear Editor,

This letter accompanies the manuscript entitled **"COPZ1 depletion in thyroid tumor cells triggers type I IFN response and immunogenic cell death"** by Di Marco T , Bianchi F, Sfondrini L, Todoerti K, Bongarzone I, Maffioli E, Tedeschi G, Mazzoni M, Pagliardini S, Pellegrini S, Neri A, Anania MC and Greco A.

We wish to confirm that there are no known conflicts of interest associated with this publication and there has been no significant financial support for this work that could have influenced its outcome.

Sincerely yours

Dr. Angela Greco
Unit "Molecular Mechanisms"
Dep. of Experimental Oncology and Molecular Medicine
Fondazione IRCCS Istituto Nazionale dei Tumori
Via GA Amadeo, 42
20133 Milan, Italy
Tel 39-0223903222
Fax 39-0223903073
e-mail angela.greco@istitutotumori.mi.it